THE JOURNAL OF BIOLOGICAL CHEMISTRY VOL. 288, NO. 6, pp. 4436–4451, February 8, 2013

Metabolism of 1-Methyl-4-phenyl-1,2,3,6-tetrahydropyridine by Mitochondrion-targeted Cytochrome P450 2D6

*IMPLICATIONS IN PARKINSON DISEASE**

Received for publication, July 20, 2012, and in revised form, November 27, 2012 Published, JBC Papers in Press, December 20, 2012, DOI 10.1074/jbc.M112.402123

Prachi Bajpai[‡1], Michelle C. Sangar[‡1], Shilpee Singh[‡], Weigang Tang[‡], Seema Bansal[‡], Goutam Chowdhury[§], Qian Cheng[§], Ji-Kang Fang[‡], Martha V. Martin[§], F. Peter Guengerich[§], and Narayan G. Avadhani[‡2]

From the [‡]Department of Animal Biology and Marie Lowe Center for Comparative Oncology, School of Veterinary Medicine, University of Pennsylvania, Philadelphia, Pennsylvania 19104-6046 and the [§]Department of Biochemistry and Center in Molecular Toxicology, School of Medicine, Vanderbilt University, Nashville, Tennessee 37232-0146

Background: Metabolism of 1-methyl-4-phenyl-1,2,3,6-tetrahydropyridine (MPTP) to toxic MPP^+ is critical in chemically induced Parkinson disease.
Results: Mitochondrial CYP2D6 supported by adrenodoxin/adrenodoxin reductase efficiently catalyzed MPTP to MPP^+.
Conclusion: Mitochondria from dopaminergic neurons contain the enzymes for the metabolism of MPTP to MPP^+.
Significance: This is a new pathway for the metabolism of MPTP to toxic MPP^+ within the dopaminergic neurons.

1-Methyl-4-phenyl-1,2,3,6-tetrahydropyridine (MPTP) is a neurotoxic side product formed in the chemical synthesis of desmethylprodine opioid analgesic, which induces Parkinson disease. Monoamine oxidase B, present in the mitochondrial outer membrane of glial cells, catalyzes the oxidation of MPTP to the toxic 1-methyl-4-phenylpyridinium ion (MPP^+), which then targets the dopaminergic neurons causing neuronal death. Here, we demonstrate that mitochondrion-targeted human cytochrome P450 2D6 (CYP2D6), supported by mitochondrial adrenodoxin and adrenodoxin reductase, can efficiently catalyze the metabolism of MPTP to MPP^+, as shown with purified enzymes and also in cells expressing mitochondrial CYP2D6. Neuro-2A cells stably expressing predominantly mitochondrion-targeted CYP2D6 were more sensitive to MPTP-mediated mitochondrial respiratory dysfunction and complex I inhibition than cells expressing predominantly endoplasmic reticulum-targeted CYP2D6. Mitochondrial CYP2D6 expressing Neuro-2A cells produced higher levels of reactive oxygen species and showed abnormal mitochondrial structures. MPTP treatment also induced mitochondrial translocation of an autophagic marker, Parkin, and a mitochondrial fission marker, Drp1, in differentiated neurons expressing mitochondrial CYP2D6. MPTP-mediated toxicity in primary dopaminergic neurons was attenuated by CYP2D6 inhibitor, quinidine, and also partly by monoamine oxidase B inhibitors deprenyl and pargyline. These studies show for the first time that dopaminergic neurons expressing mitochondrial CYP2D6 are fully capable of activating the pro-neurotoxin MPTP and inducing neuronal damage, which is effectively prevented by the CYP2D6 inhibitor quinidine.

1-Methyl-4-phenyl-1,2,3,6-tetrahydropyridine (MPTP),[3] a contaminant in synthetic heroin (a "designer drug"), is a neurotoxin and induces Parkinson-like syndrome in humans, nonhuman primates, and mice (1–3). This compound has been used as a valuable model substance for investigating mechanisms of Parkinson disease for >30 years. MPTP is a pro-toxin, and current models suggest that the neurotoxin crosses the blood-brain barrier following systemic administration and is oxidized to $MPDP^+$ by monoamine oxidase (MAO) B, localized on the mitochondrial outer membrane of nondopaminergic cells (4). $MPDP^+$ is an unstable compound that undergoes further oxidation to form the active toxic compound MPP^+ (5). MPP^+ is far less lipophilic than MPTP and cannot easily diffuse across cellular membrane lipid bilayers (6), but it is actively transported inside dopaminergic neurons by the dopamine transporter (7). Within the dopaminergic neurons, MPP^+ sequesters inside the mitochondrial compartment because of the positive charge it carries (8) and preferentially binds to and inhibits complex I of the electron transport chain (9). Inhibition of complex I leading to lower ATP generation (10), increased production of reactive oxygen species (ROS) (11, 12), and eventual cell death are believed to be the steps leading to Parkinson disease (13).

Although MAO-B from glial cells is believed to be the main enzyme involved in the bioactivation of MPTP, cytochrome P450 2D6 (CYP2D6) is localized in the dopaminergic neurons of the substantia nigra (14) and has been suggested to be an important player in determining MPTP toxicity. This enzyme has been considered to be involved in detoxification because of

* This work was supported, in whole or in part, by National Institutes of Health Grant R01 GM034883, Grant R37 CA090426 (to F. P. G.), and Training Grant T32 GM007170 (to M. C. S.). This work was also supported by an American Recovery Act supplement and by a Harriet Ellison Woodward endowment (to N. G. A.).
[1] Both authors contributed equally to this work.
[2] To whom correspondence should be addressed. Tel.: 215-898-8819; Fax: 215-573-6810; E-mail: Narayan@vet.upenn.edu.

[3] The abbreviations used are: MPTP, 1-methyl-4-phenyl-1,2,3,6-tetrahydropyridine; CYP2D6, cytochrome P450 2D6; Adx, adrenodoxin; Adr, NADPH-adrenodoxin reductase; NPR, NADPH-cytochrome P450 reductase; OCR, oxygen consumption rates; ROS, reactive oxygen species; MAO, monamine oxidase. MPP^+, 1-methyl-4-phenyl pyridinium ion; TH, tyrosine hydroxylase; SRP, signal recognition particle; PTP, 4-phenyl-1,2,3,6-tetrahydropyridinium ion; MPDP, 1-methyl 4-phenyl 2–3-dihydropyridinium ion; ER, endoplasmic reticulum; DNP, 2,4-dinitrophenol; CYP, cytochrome P450.

its demonstrated ability to catalyze *N*-demethylation and *p*-hydroxylation of MPTP to form inactive products (15–20). Microsomal CYP2D6 has also been shown to catalyze the oxidative dehydrogenation of MPTP to form MPP^+, albeit less efficiently than MAO-B (18). Therefore, the delineation between enzymes that activate and those that inactivate may not be as clear as once thought. It is also possible that polymorphisms in *CYP2D6* could affect the extent of MPTP metabolism as well as the nature of the metabolites, as there have been several reports of substrate-specific activity profiles for *CYP2D6* variant alleles (19). Of the >112 *CYP2D6* polymorphisms reported thus far, several have been shown to be clinically significant by altering enzyme activity, thereby affecting drug efficacy and toxicity. It is not clear how polymorphic forms of *CYP2D6* affect MPTP toxicity or detoxification.

CYP2D6 is predominantly localized in the microsomal membrane fractions of the liver, brain, and other peripheral tissues. Several epidemiological investigations have suggested concordance between *CYP2D6* gene polymorphism and the incidence of Parkinson disease (20–22); however, other studies have shown no such association (23–25). Furthermore, studies in our laboratory showed that members of CYP2 family, including CYP2D6, are also targeted to mitochondria, and human livers showed marked variations in mitochondrial CYP2D6 (26, 27). In some cases, the mitochondrial concentration was higher than the microsomal content (26). Additionally, studies with CYP1A1, -2B1, and -2E1 showed some significant difference in the substrate specificity and catalytic activities of the mitochondrially localized enzymes compared with their microsomal counterparts (28). In this study, we investigated the ability of human CYP2D6 targeted to the mitochondrial compartment of COS-7 and mouse Neuro-2A cells to metabolize MPTP, and we found that the mitochondrial enzyme supported by Adx and Adr electron transfer proteins catalyzes the bioactivation of MPTP to toxic MPP^+ with efficiency comparable with MAO-B. Our results show that dopaminergic neurons contain full capability for the bioactivation of MPTP to toxic MPP^+, which causes mitochondrial complex I inhibition and neuronal damage.

MATERIALS AND METHODS

Cell Lines and Culture Conditions—COS-7 fibroblasts (ATCC CRL-1651) and mouse Neuro-2A cells (ATCC CCL-131) were grown in Dulbecco's modified Eagle's medium (DMEM) (Invitrogen) supplemented with 10% fetal bovine serum (v/v) and 0.1% gentamycin (w/v). Generation of a doxycycline-inducible cell line was reported previously (26). Stable Neuro-2A cells were generated by transducing with *CYP2D6* cDNAs cloned in a retroviral vector (pBABE-puro), and stable clones were selected based on resistance to puromycin. Viral particles for transduction were prepared in 293T cells by co-transfection with gag-pol and VSV-G plasmids (29). Puromycin was added after every two passages to ensure the integrity of the viral vectors. All the experiments were conducted in the cells that were cultured without puromycin for at least three passages to rule out the adverse effects of puromycin on mitochondrial function. In differentiation studies, medium was changed to DMEM with 0.5% FBS (differentiation medium, v/v) after overnight growth and grown for an additional 3 days with 1 mM Bt_2cAMP (Sigma).

Preparation and Treatment of Primary Neurons—Primary neurons were prepared from cortices and mesencephali of *C57BL*/6 mouse brains at gestation day 16/17. The isolated tissue was mechanically dissociated and digested with 1 mg/ml of papain (Worthington) for 15 min at 34 °C followed by addition of 3 μg/ml DNase I (Roche Diagnostics) for 5 min. The suspension was triturated, passed through a 70-μm strainer, and centrifuged at 250 × *g* for 8 min. Pellet was resuspended in Dulbecco's phosphate-buffered saline containing 30 μg/ml DNase I and centrifuged. Finally, the pellet was washed, resuspended in Neurobasal medium supplemented with 2% (v/v) B-27 supplement, 0.5 mM L-glutamine (GlutaMAX^{TM}, Invitrogen), and seeded on poly-D-lysine ((P899, Sigma)-coated coverslips at $8 \times 10^4/cm^2$. The culture was maintained at 37 °C in humidified 95% air, 5% CO_2 (v/v) incubator. This procedure typically yields neuron-enriched cultures containing >98% neurons. In the case of mesencephalic neurons, 3–4% were dopaminergic (TH-positive) cells. On the 8th day in culture (DIV8), neurons were treated with 50 μM MPTP with and without 10 μM quinidine, 5 μM pargyline, or 10 μM deprenyl for 48 h.

Isolation of Mitochondria from Different Cell Lines—Mitochondria were isolated by differential centrifugation of cell homogenates as described previously (26), using a sucrose/mannitol buffer (20 mM HEPES, pH 7.5, containing 70 mM sucrose, 220 mM mannitol, and 2 mM EDTA). Crude mitochondria, resuspended in sucrose/mannitol buffer, were sedimented through a layer of 0.8 M sucrose by centrifugation at 14,000 × *g* for 20 min. The pellet was then washed with sucrose/mannitol buffer. When used for metabolic assays, the final mitochondrial pellet was resuspended in 50 mM potassium phosphate buffer, pH 7.5, containing 20% glycerol (v/v), 0.1 mM EDTA, 0.1 mM dithiothreitol, and 0.1 mM phenylmethylsulfonyl fluoride. For other analyses, mitochondria were resuspended in the sucrose/mannitol buffer containing leupeptin (1 μg/ml) and pepstatin (1 μg/ml).

Measurements of MAO Activity—Mitochondria were assayed for MAO activity using kynuramine as a substrate (30) fluorometrically by either using a Photon Technology International spectrofluorometer or a Chameleon Multilabel Detection Platform. Reactions were performed in a final volume of 1.5 ml of 75 mM potassium phosphate buffer, pH 7.4, containing 150 μM kynuramine and 250 μg of mitochondrial protein at 37 °C for 30 min in a shaking water bath. Trichloroacetic acid (1 ml, 10% w/v) was added to terminate the reactions, and 0.5 ml of the clarified supernatant ($10^3 \times g$ for 10 min) was mixed with 1 ml of 1 M NaOH. Measurements (of the product) were made in an 814 PMT spectrofluorometer (PTI, Birmingham, NJ), with 315 nm extinction and 380 nm emission. Inhibition studies were performed by preincubating mitochondria with deprenyl (20 μM) or clorgyline (20 μM) for 10 min on ice before addition to the reaction mixture.

Fluorometric assays of MAO-A/B (total for the two enzyme) were done using a Fluoro:MAO detection kit (Cell Technology, CA) following the manufacturer's protocol. Mitochondria (10 μg of protein) was taken for analysis with and without inhibitors in 100 μl of Reaction Mixture in a black 96-well plate. For

detection of MAO-B activity, benzylamine was used as the substrate and inhibited by 10 μM pargyline; similarly for MAO-A activity, tyramine was used as the substrate and inhibited by 10 μM clorgyline (data not shown). In addition to the mitochondria of Neuro-2A cells, mitochondria from rat brain and C6 glioma were tested as positive controls. Plates were incubated in the dark at 37 °C for 30 min, and readings were taken using a Microwin Chameleon microplate reader, with excitation at 530 nm and an emission wavelength of 590 nm.

Immunoblot Analysis of Proteins—Protein estimation was done by the method of Lowry *et al.* (31). Mitochondrial proteins (50 μg) were resolved by SDS-PAGE and transferred to supported nitrocellulose membranes (Bio-Rad). A CYP2D6 monoclonal antibody was used at a dilution of 1:500 (v/v, BD Gentest, BD Biosciences). A tyrosine hydroxylase monoclonal antibody was used at a dilution of 1:2000 (v/v, Immuno StAR, Hudson, WI). Blots for cell lysate were co-developed with antibody to succinate dehydrogenase (1:5000 dilution, v/v; Abcam, Cambridge, MA) or actin (1:5000 dilution, v/v; Abcam, Cambridge, MA) as loading control. To evaluate microsomal and mitochondrial cross-contamination, blots were co-developed with antibodies to NPR (1:1500 dilution, v/v; Santa Cruz Biotechnology), TOM20 (1:1500 dilution, v/v; Santa Cruz Biotechnology), and 1:50,000 dilutions (v/v) of infrared dye-conjugated secondary antibodies. Blots were probed and developed using the SuperSignal West Femto System (Pierce) and imaged on a Bio-Rad VersaDoc Imaging System or Odyssey LICOR instrument (LICOR Biotechnology, Lincoln, NE). Digital image analysis was performed using Quantity One Version 4.5 software from Bio-Rad.

Analysis of Cellular O_2 Consumption by Respirometry—Oxygen consumption rates (OCR) were measured using a XF24 high sensitivity respirometer (Seahorse Bioscience) as described by Wu *et al.* (32), following the manufacturer's instructions. Neuro-2A cells were cultured in Dulbecco's modified Eagle's medium (DMEM) without and with MPTP (400 μM). In each case, 25,000 cells were cultured in DMEM overnight and changed with XF assay medium, low buffered bicarbonate-free DMEM, pH 7.4, for 1 h before the measurement. The final concentrations of inhibitors used were 2 μg/ml oligomycin, 40 μM 2,4-dinitrophenol (DNP, used as uncoupler), and 1 μM complex I inhibitor rotenone. Each plate (along with the cartridge) was loaded into the XF analyzer. OCR was measured under basal conditions and after the sequential addition of oligomycin, DNP, and rotenone. All respiration rates were calculated as percentage of the rate. Respiration rates at each time point from three replicate wells were averaged.

Oxidation Assays with MPTP and Bufuralol—Purified CYP2D6, isolated mitochondria, and microsomes from cell lines were assayed for oxidation of MPTP and bufuralol using optimal assay conditions described before (17, 58, 60). As described before (58, 60), reconstitution with Adx and Adr was carried out without added liposomes, whereas that with NPR was carried with phospholipid vesicles. Reactions were carried out in 0.2 ml (final volume) of 75 mM sodium phosphate buffer, pH 7.4, containing 300 μg of mitochondrial protein or 300 μg of microsomal protein. Mitochondrial enzyme and purified CYP2D6 (0.1 nmol) were reconstituted with 0.2 nmol of purified Adx, 0.02 nmol of purified Adr, or 0.2 nmol of purified NPR and 400 μM MPTP. Mitochondria were frozen and thawed four times in a hypotonic buffer (25 mM sodium phosphate buffer, pH 7.2) to permeabilize the membranes before addition to the reaction mixtures. Inhibition studies were performed by preincubating enzymes for 10 min on ice with 10 μl of CYP2D6 of inhibitory antibody (10 mg/ml, BD Gentest, BD Biosciences), 10 μM quinidine, or 5–20 μM deprenyl (Sigma). Reactions were initiated by addition of 50 μl of 4 mM NADPH and incubated for 15 min at 37 °C in a shaking water bath. Reactions were terminated by addition of 50 μl of a $HClO_4/CH_3OH$ mixture (1:1, v/v), mixed using a vortex device, and centrifuged at 9000 $\times$ *g* for 20 min at 4 °C. The supernatants were analyzed by LC/MS.

Bufuralol oxidation assays were carried out as described by Hanna *et al.* (17) using 100 pmol of purified CYP2D6, 250 μg of microsomal protein, or 300 μg of mitochondrial protein from CYP2D6-expressing cell lines, using conditions essentially as described for MPTP. The mixtures were preincubated for 3 min at 37 °C, and then 120 μM NADPH was added to initiate the reactions. Incubations were carried out for 10 min and then quenched by addition of 25 μl of 60% $HClO_4$ (w/v). Reaction mixtures were centrifuged at 3000 $\times$ *g* for 10 min, and the supernatants were analyzed by LC/MS. For all P450-mediated assays, quinidine was added from a stock solution in DMSO. The same volume (10 ml) of DMSO was added to control reactions. Other inhibitors were added as stocks in distilled water.

LC/MS Analysis of MPTP Products—Samples were analyzed by LCMS using a TSQ quantum mass spectrometer with a CERI L-column 2 octadecylsilane column (2.1 $\times$ 150 mm, 5 μm, CERI, Tokyo, Japan). LC conditions were as follow: solvent A contained 95% (v/v) H_2O and 5% (v/v) CH_3CN with 0.1% (v/v) HCO_2H, and solvent B contained 95% (v/v) CH_3CN and 5% (v/v) H_2O with 0.1% HCO_2H. The column was maintained at 20% (v/v) solvent B with a flow rate of 300 μl/min. Data acquisition was performed in the positive ESI mode using selected reaction monitoring as follows: *m/z* 174 $\rightarrow$ 91 for MPTP, *m/z* 172 $\rightarrow$ 115 for $MPDP^+$, *m/z* 170 $\rightarrow$ 128 for MPP^+, and *m/z* 190 $\rightarrow$ 85 for MPTP-OH.

LC/MS Analysis of Bufuralol Metabolites—Samples were analyzed in an ESI linear trap ion mass spectrometer (LTQ, Thermo-Fisher, San Jose, CA) connected to a Waters Acquity UPLC system (Waters, Milford, MA) using an Acquity UPLC BEH Shield octadecylsilane (RP18) column (1.7 μm, 1.0 $\times$ 100 mm). LC conditions were as follows: buffer A contained 0.1% HCO_2H (v/v) in H_2O, and buffer B contained 0.1% HCO_2H (v/v) in CH_3CN (v/v). The following gradient program was used with a flow rate of 150 μl/min: 0–6 min, linear gradient from 5 to 80% B (v/v); 6–6.5 min, linear gradient to 100% B; 6.5–7.5 min, hold at 100% B; 7.5–8.5 min, linear gradient to 95% A (v/v); 8–10 min, hold at 95% A (v/v). The temperature of the column was maintained at 25 °C. Samples (20 μl) were infused with an auto-sampler. ESI conditions were as follows: source voltage 3.5 kV, source current 100 μA, auxiliary gas flow rate setting 12, sheath gas flow setting 43, capillary voltage 20 V, capillary temperature 300 °C, tube lens voltage 45 V. Two transitions, *m/z* 278 $\rightarrow$ 242 and 278 $\rightarrow$ 186, were used to monitor 1′-hydroxybufuralol formation. MSMS conditions were as follows: nor-

malized collision energy 30%, activation *Q* 0.250, and activation time 30 ms.

Measurement of Mitochondrial Complex I Activity—Complex I activity was assayed as described by Birch-Machin and Turnbull (33) with modifications, using a NanoDrop 2000c spectrophotometer (Thermo Scientific, Waltham, MA), and the decrease in absorbance at 340 nm was recorded for 3 min, indicating the extent of NADH oxidation ($slope_1$). Rotenone (5 μg/ml) was added to each reaction, and the absorbance was measured at 340 nm for another 2 min ($slope_2$). The rotenone sensitive activity ($slope_1 - slope_2$) was used to calculate the final complex I activity for each sample.

Bacterial Expression and Purification of Human CYP2D6—CYP2D6 (construct DB6, with a C-terminal His_6 tag) was expressed in *Escherichia coli* and purified as described earlier (17). Recombinant *E. coli* rat NPR was expressed and purified as described (34).

Quantitative Real Time PCR—Total DNA was isolated from cells using DNeasy blood and tissue kit in accordance with the manufacturer's instructions (Qiagen, CA). The vector DNA integrated in the genome was determined with using puromycin acetyltransferase gene of the vector construct in relation to nuclear CcO Vb DNA used as an internal control.

Total RNA was isolated from cells using TRIzol reagent in accordance with the manufacturer's instructions (Invitrogen). The levels of the integrated puromycin resistance RNA in relation to cellular β-actin used as a control were determined. For real time PCR analysis, 1 μg of total RNA was reverse-transcribed using the high capacity cDNA archive kit (Applied Biosystems), and 50 ng of the resulting cDNA was used in standard Power SYBR Green real time PCR on an ABI 7300 real time PCR machine and analyzed using Primer Express 3.0 (Applied Biosystems).

Measurement of Extracellular H_2O_2 by Amplex Red—H_2O_2 in cells (hereafter referred to as ROS) was measured using the Amplex Red hydrogen peroxide/peroxidase assay kit from Invitrogen. For measurement in whole cells, 25×10^3 cells, pretreated with various antioxidants or inhibitors, were seeded in a 96-well black bottom plate in phenol-free medium and incubated at 37 °C for 4 h for cells to adhere, followed by the incubations with HRP and Amplex Red (10 mM) in PBS for 15 min at 37 °C. The method involves the horseradish peroxidase (HRP)-catalyzed oxidation of the colorless and nonfluorescent molecule, *N*-acetyl-3,7-dihydroxyphenoxazine (Amplex Red) to resorufin. The fluorescence was recorded at an excitation of 530 nm and emission at 590 nm in a MicroWin chameleon multilabel detection platform. Superoxide dismutase (from bovine erythrocytes, Sigma) and catalase (from bovine liver, Sigma) were added to 100 and 500 units/ml, respectively. Membrane-permeable superoxide dismutase and catalase were used for assessing specificity of the signal.

Immunofluorescence Microscopy—Cells were fixed with methanol, permeabilized by 0.1% Triton X-100 (v/v), blocked with 5% goat serum (v/v), and stained with appropriate primary and secondary antibodies. Fluorescence microscopy was done using Olympus BX61 microscope, and the Pearson's coefficient was calculated using Volocity 5.3 software.

Measurement of Cytochrome P450 Content—The CYP contents of mitochondrial and microsomal membranes were measured by the difference spectra of CO-treated and dithionite-reduced samples as described by Omura and Sato (35), and as modified by Guengerich (36), using a dual-beam spectrophotometer (Cary 1E; Varian, Walnut Creek, CA). Mitochondrial or microsomal (0.5 mg) proteins were solubilized in potassium phosphate buffer (0.1 M, pH 7.4) containing 1 mM EDTA, 20% glycerol (v/v), sodium cholate (0.5%, w/v), and Triton N-101 (0.4%, w/v). Sodium hydrosulfite (dithionite) was added and the base line was recorded. The solution in the sample cuvette was then bubbled gently with CO for 60 s. The spectrum was recorded in the range 400–500 nm. The P450 contents were calculated as described (35).

Quantification of Trypan Blue-positive and TH-immunoreactive Cells—To assess cell death, cortical neurons were stained with 0.4% trypan blue (w/v) for 15 min. Positive trypan blue staining indicates damaged membrane and loss of cell viability. Neuronal cell death was calculated by counting trypan blue-positive cells in six random fields per well at ×20 magnification using light microscopy (Nikon Eclipse TE300) and expressed as a percentage of total number of neurons. To quantify TH-positive cells, mesencephalic neurons showing TH immunoreactivity were observed on each coverslip. The coverslip was delineated into nine frames and systematically counted both at ×10 and ×40 magnification using an Olympus BX61 microscope, equipped with Metamorph Advanced Software. Only cells with distinct immunoreactivity and clearly visible cell body were counted from three independent experiments, averaged, and presented as percentage of control.

Statistical Analysis—The means ± S.D. were calculated from three to five experimental values. *p* values were calculated using a one-tailed equal variance *t* test when compared with MPTP (compared with no MPTP) and unequal variance when a *t* test was used to calculate significance with MPTP treatment with different groups.

RESULTS

Metabolism of MPTP by Mitochondria in CYP2D6-expressing COS Cells—We previously expressed WT and mutant *CYP2D6* cDNAs with altered targeting signals (26, 37) using a doxycycline (Dox)-inducible lentiviral vector LVPT-tTRKRAB (26) in COS cells. Because our objective was to delineate the roles of MAO and mitochondrial CYP2D6 in the metabolism of the neurotoxin MPTP, we assessed the MAO activities in COS cell mitochondria in comparison with brain mitochondria. The total MAO activity of brain mitochondria was approximately four times higher than in COS cell mitochondria (Fig. 1*A*). MAO-A activity in COS cell mitochondria was about 5-fold higher than MAO-B activity, as indicated by relative inhibition by deprenyl (a MAO-B inhibitor) and chlorgyline (a MAO-A inhibitor). We therefore used mitochondria from stably expressing COS cells to test the ability of mitochondrion-targeted CYP2D6 to oxidize MPTP.

The immunochemical analysis of total cell lysates showed that the CYP2D6 protein was induced by Dox only in cells transduced with WT *CYP2D6* cDNA containing vector and that mock-transfected cells did not show any detectable

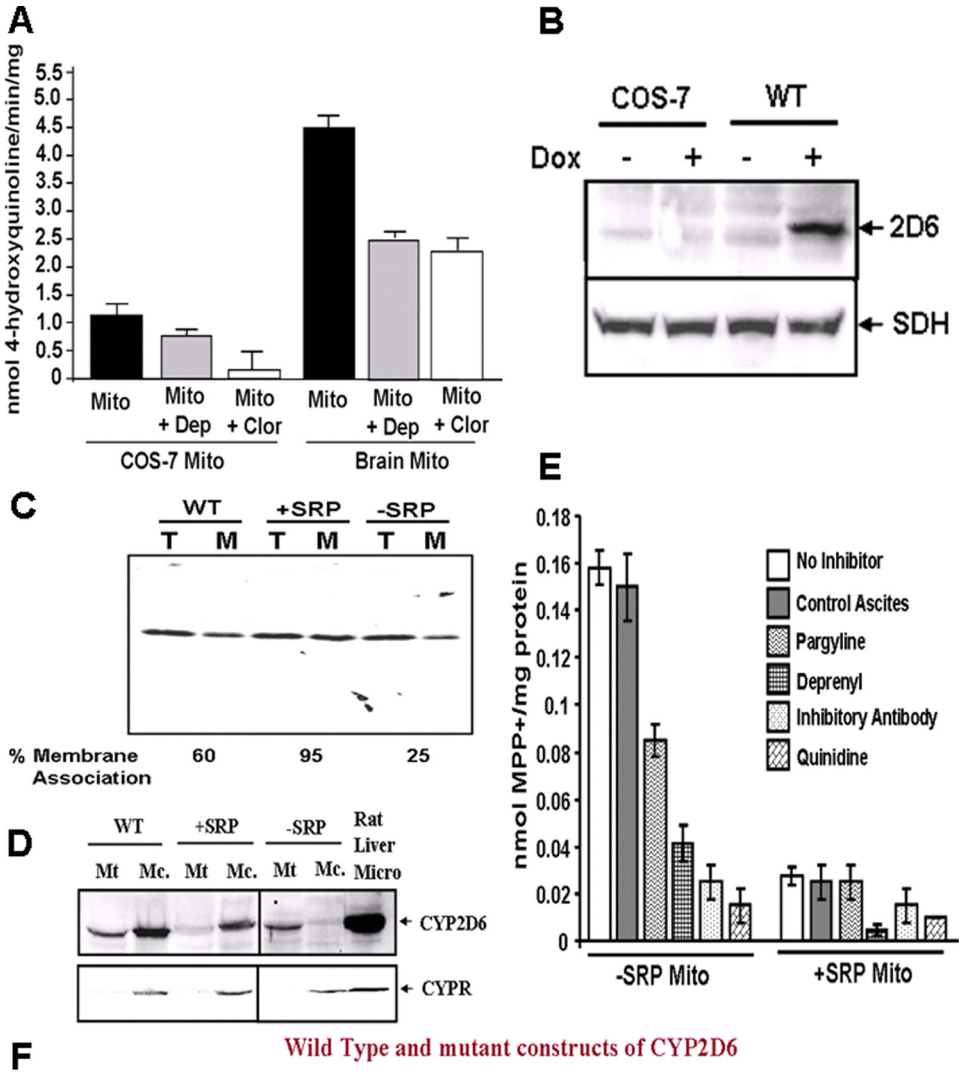

FIGURE 1. **Oxidation of MPTP by mitochondrial and ER-targeted human CYP2D6.** *A*, MAO activities of mitochondrial preparations from COS-7 cells mock-transfected with Dox-inducible lentiviral vector and mouse brain mitochondria. Metabolism of kynuramine to 4-hydroxyquinoline was carried out as described under "Materials and Methods" using isolated mitochondria. Mitochondria (*Mito*) were preincubated with or without added inhibitors (deprenyl (*Dep*) or chlorgyline (*Clor*), 20 μM each) for 10 min on ice before starting the assay. Means ± S.E. are shown ($n = 3$). *B*, immunoblots of whole cell extracts (50 μg each) from COS-7 cells expressing WT CYP2D6 treated with or without Dox (to induce CYP2D6). The blot was also developed with antibody to succinate dehydrogenase (*SDH*) to assess loading levels. *C*, ER membrane integration assay; the SRP binding affinities of WT, +SRP, and −SRP proteins were performed as described under "Materials and Methods." The method essentially tests the extent of integration of labeled nascent proteins into unwashed canine pancreatic ER membrane. *T*, total translation product used in the assay; *M*, proteins bound to the ER membrane fraction that was re-isolated and washed. Proteins were analyzed by SDS-PAGE and subjected to autoradiography. Radiometric analysis was performed to determine the percentage of the total translation product that associated with the ER membrane for each construct. *D*, mitochondrial (*Mt*) and microsomal (*Mc*) CYP2D6 levels in WT, −SRP, and +SRP CYP2D6-expressing cells (induced with Dox). A rat liver microsomal (*Micro*) sample was used as a positive control. Proteins (30 μg each) were subjected to immunoblot analysis as described under "Materials and Methods." The blot was developed with a monoclonal antibody to human CYP2D6 (1:1000 dilution, v/v) and co-developed with NPR antibody (1:1500 dilution, v/v) to assess levels of microsomal contamination of mitochondrial preparations. *E*, oxidation of MPTP by mitochondria from Dox-induced COS-7 cells expressing −SRP and +SRP CYP2D6. The oxidation products were quantified by nano-LC-MS-MS analysis as described under "Materials and Methods." A standard curve of MPP$^+$ was used to calculate moles of MPP$^+$ formed per mg of protein. Inhibition studies were performed by preincubating enzymes for 20 min on ice with 10 μl of CYP2D6 inhibitory antibody or control ascites protein (10 mg/ml, BD Gentest, BD Biosciences) or 10 μM quinidine and 10 μM pargyline and 10 μM deprenyl at 37 °C for 20 min. *F*, schematic representation of WT2D6 and its mutant constructs. Mutated amino acids are *underlined*.

CYP2D6 even after Dox treatment (Fig. 1*B*). The +SRP mutant carries more hydrophobic substitutions within the N-terminal signal region and is predicted to have higher affinity for SRP binding and higher microsomal targeting. The −SRP mutant carries more hydrophilic mutations and is therefore predicted to have lower affinity for SRP binding and higher mitochondrion-targeting efficiency. The N-terminal signal domains and the −SRP and +SRP mutations are shown in Fig. 1*F*. The SRP binding efficiency of WT and mutant protein was tested using a membrane integration assay described before (57). It is seen

that close to 60% of the WT nascent chains associated with the added unwashed canine pancreatic ER, which was increased to 95% for the +SRP CYP2D6 protein (Fig. 1*C*). As predicted, the −SRP CYP2D6 protein with more hydrophilic residues in the N-terminal signal region bound to the ER at a reduced efficiency of 25% (Fig. 1*C*). The mitochondrial and microsomal distributions of CYP2D6 in Dox-induced cells expressing human WT, +SRP, and −SRP *CYP2D6* cDNAs are shown in Fig. 1*D*. It is seen that only about 25% of WT CYP2D6 was targeted to mitochondria (Fig. 1*D*). Both the −SRP and +SRP mutant constructs exhibited a marginally lower level of expression of CYP2D6 than the WT construct, although the +SRP mutant was preferentially targeted to microsomes, and −SRP mutant was preferentially targeted to mitochondria (Fig. 1*D*). These results support the hypothesis that the SRP binding efficiency is a rate-limiting factor in the targeting of nascent chains to microsomes or mitochondria.

The oxidation products of MPTP formed by isolated mitochondria from −SRP and +SRP 2D6-expressing cells induced with Dox were analyzed by LC/MS with added internal controls and co-elution with MPP+ run as a standard. The results on formation of MPP^+ with isolated mitochondria are summarized in Fig. 1*E*. Mitochondria from −SRP CYP2D6-expressing cells showed a high level of toxic MPP^+ formation (0.16 nmol/mg protein), which was not inhibited by control ascites protein but inhibited about 65% by a CYP2D6-specific antibody. The activity was inhibited by a CYP2D6-specific inhibitor quinidine further suggesting that most of the metabolic activity was due to CYP2D6. The known MAO-B inhibitors deprenyl and pargyline inhibited the activity by 90 and 45%, respectively. Mitochondria from +SRP CYP2D6-expressing cells showed nearly 10-fold lower activity, which was partly inhibited by CYP2D6 antibody, deprenyl and quinidine. Our data support previous studies showing that deprenyl is a known substrate for CYP2D6 (38), but inhibition by pargyline was surprising. These results suggested the possibility that deprenyl and pargyline inhibit both CYP2D6-dependent as well as MAO-dependent metabolism of MPTP to MPP^+. The relative MPTP metabolic activities in −SRP CYP2D6- and +SRP CYP2D6-expressing cells were consistent with the mitochondrial CYP2D6 levels observed in Fig. 1*D*. Additionally, the CYP contents of mitochondrial preparations in these two cases differed nearly 10-fold with −SRP CYP2D6 mitochondria showing about 0.2 nmol of CYP content/mg of protein.

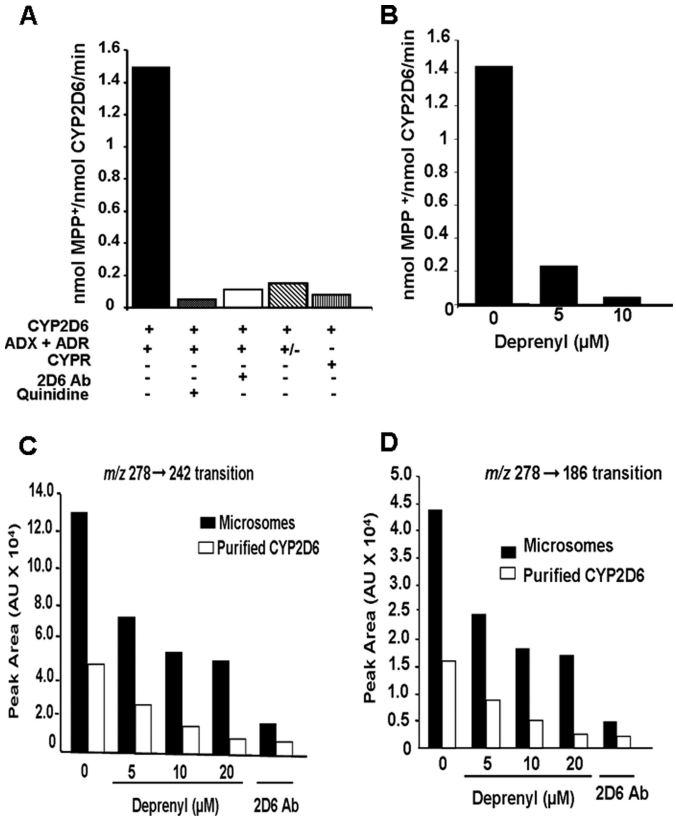

FIGURE 2. **Oxidation of MPTP and bufuralol by purified CYP2D6 reconstituted with Adx and AdxR.** CYP2D6-purified enzyme was reconstituted with mitochondrial electron transfer proteins, Adx and AdxR, or microsomal electron transfer protein NPR in the presence or absence of added inhibitors as described under "Materials and Methods." *A*, levels of MPP^+ formed were quantified using an LC-MS method as described under "Materials and Methods." The control sample in *A* was treated with 10 μl of ascites fluid (10 mg/ml), and the corresponding control without treatment with ascites is presented in *B*. In the indicated reactions, the CYP2D6 antibody was added at 10 μg/reaction, and quinidine was added at 10 μM. In the reaction marked "+/−", Adr was omitted from the assay mixture. The value for MPP^+ formed in each case represents the mean ± S.E. for three separate estimates. *B*, effects of increasing concentrations of deprenyl (5 and 10 μM) on MPTP metabolism was tested. *In vitro* reactions with purified CYP2D6 were run, and the MPP^+ metabolite was quantified as described under "Materials and Methods." *C* and *D*, microsomes from −SRP CYP2D6-expressing cells (200 μg each) and purified CYP2D6 reconstituted with Adx and Adr as in described in Fig. 1 and under "Materials and Methods" were used for bufuralol oxidation assays, and the products were subjected to LC/MS/MS analysis. The indicated concentrations of deprenyl were added to reactions. In one assay, 10 μg of CYP2D6 antibody was added. 1′-Hydroxybufuralol was monitored using two transitions, *m/z* 278 → 242 and *m/z* 278 → 186.

Oxidation of MPTP by Purified CYP2D6—The ability of CYP2D6 to oxidize the pro-neurotoxin MPTP to toxic MPP^+ and the possible inhibitory effect of deprenyl on CYP2D6-dependent metabolism was investigated using purified CYP2D6 reconstituted with Adx + Adr and NPR electron transfer systems. Recombinant purified human CYP2D6 actively metabolized MPTP to MPP^+ in an Adx/Adr-supported system (Fig. 2*A*). As in the case of reactions with isolated mitochondria, MPP^+ (*m/z* 170 → 128) was the major product formed, and there was negligible PTP (*m/z* 160) or MPTP-OH (*m/z* 190). Reactions with added control ascites protein yielded maximum activity, which was comparable with no ascites control (Fig. 2*B*). Quinidine, a CYP2D6-selective inhibitor and CYP2D6-specific inhibitory antibody, inhibited the activity by <85%. Similarly, omission of Adr from the reaction mixture brought down the activity by >80% (Fig. 2*A*). In agreement with previous reports (18), purified CYP2D6 yielded a very low level of MPP^+ in an NPR-supported system, ~6% of the amount in the Adx + Adr-supported system. These results suggest a major difference in the metabolic activity of the enzyme supported with two different electron donor systems. Deprenyl inhibited the Adx + Adr-supported oxidation of MPTP by purified CYP2D6, in a concentration-dependent manner (Fig. 2*B*). Deprenyl also inhibited the bufuralol 1′-hydroxylation activity of microsomes from +SRP CYP2D6-expressing cells and purified CYP2D6 reconstituted with Adx + Adr in a concentration-dependent manner (Fig. 2, *C* and *D*). Thus, inhibition of CYP2D6 activity by deprenyl is not restricted to a single substrate. Although not

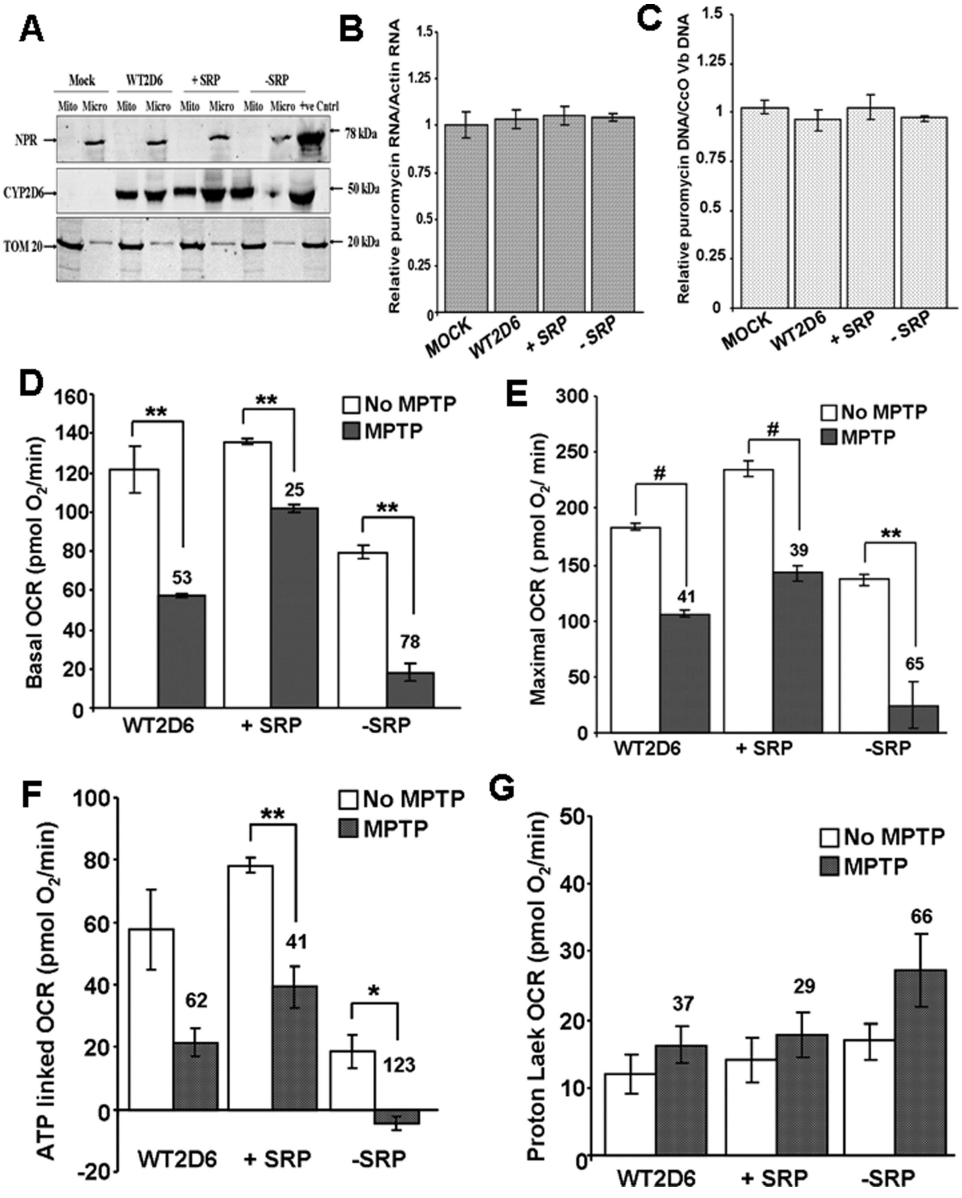

FIGURE 3. **Effects of MPTP on Neuro-2A cells stably expressing different *CYP2D6* cDNA constructs.** *A*, mitochondrial (*Mito*) and microsomal (*Micro*) isolates from Neuro-2A cells stably transduced with adenoviral vector with cloned WT, −SRP, and +SRP *CYP2D6* cDNAs were subjected to immunoblot analysis; 30 μg of protein was run in each lane. The blot was co-developed with NPR antibody and TOM20 antibody. *B* and *C*, relative levels of puromycin acetyltransferase mRNA, which is the selection marker for the isolation of transduced cells, and the levels of integrated puromycin acetyltransferase gene were quantified to assess the levels of integration of vector DNA in each cell line. Actin mRNA level was used as internal control for mRNA levels, and CcO Vb gene was used as internal control for DNA level. *D–G*, respiration profile was measured in 25,000 cells using Seahorse Bioscience XF24 extracellular analyzer. All parameters were analyzed using XF software and displayed as oxygen consumption rates (pmol O_2/min/well). *D*, basal OCR accounts for base-line rates of oxygen consumption. Oligomycin (2 μg/ml), DNP (40 μM), and rotenone (1 μM) were injected through ports A–C respectively. *E*, DNP-mediated uncoupling generates maximal OCR. *F* and *G*, inhibition by oligomycin and rotenone corresponds to ATP-linked OCR and proton leak, respectively. The *number* above the bar in the *histogram* indicates % inhibition or elevation. Mean values ± S.D. were calculated based on three separate measurements. ** denotes $p < 0.05$; # denotes $p < 0.001$.

shown, pargyline also inhibited CYP2D6-dependent activity, although to a lesser extent than deprenyl (results not shown). Our results demonstrate that CYP2D6 can efficiently oxidize MPTP to yield toxic MPP$^+$ in an Adx/Adr-supported system and that the activity is also inhibited by some of the known MAO-B inhibitors.

Respiratory Patterns of Mouse Neuro-2A Cells Expressing Various CYP2D6 Forms—To evaluate the pathophysiological implications of CYP2D6 forms targeted to different cell compartments, we generated murine Neuro-2A cells that stably express different forms of CYP2D6. Because Dox is known to affect mitochondrial respiratory function in some cells, we used the retroviral vector pBABE, in which expression was driven by viral LTR for generating stable cells (39). The −SRP and +SRP mutations were similar to those described in Fig. 1*F* and previously (26, 37). The levels of mitochondrial proteins in both WT and +SRP CYP2D6-expressing cells (Fig. 3*A*) were significantly higher than seen with an inducible lentiviral system (Fig. 1). This difference may be due to the constitutive expression of the enzyme in the retroviral system. The genome-integrated marker mRNA levels for puromycin acetyltransferase was identical suggesting a similar level of expression, and also, the levels

TABLE 1

Quantification of MPTP metabolites in mitochondria from Neuro-2A cells stably transduced with human *CYP2D6* cDNA constructs

Assays were run with mitochondrial proteins from different cell lines, and the metabolites were identified by LC/MS as described under "Materials and Methods" using appropriate internal markers and standard curves for converting peak areas to molar concentration of metabolites.

Constructs	Nanomoles of metabolite/mg of protein				
	MPTP	MPDP	MPP^+	MPTP-OH	PTP
Mock	70.29	0.39	0.1	0.1	0.1
WT2D6	94.05	3.56	0.59	0.2	0.1
+SRP 2D6	89.1	0.2	0.06	0.06	0.06
−SRP 2D6	113.85	7.62	1.28	0.01	0.1
Rat brain mitochondria	82.1	30.69	3.56	0.29	0.08

of integrated vector DNA were nearly same suggesting a similar level of genome integration and possibly expression (Fig. 3, *B* and *C*).

Analysis of respiratory pattern using a SeaHorse flux analyzer shows that the basal OCR, ATP production, and maximal respiration (Fig. 3, *D–G*) were marginally increased in +SRP CYP2D6-expressing cells compared with WT CYP2D6-expressing cells. The proton leak OCR was nearly same as WT CYP2D6-expressing cells. All these functional parameters were significantly lower in −SRP 2D6-expressing cells. MPTP addition inhibited basal OCR, ATP production, and maximal OCR in all cells, although proton leakage was increased by adding MPTP mostly in −SRP 2D6-expressing cells. A notable difference was that that MPTP-induced changes were relatively modest in WT and +SRP CYP2D6-expressing cells (Fig. 3, *D–G*), although there were marked changes in −SRP CYP2D6-expressing cells.

Metabolic Activities of the WT and Mutant CYP2D6—Consistent with the severe respiratory defects in −SRP CYP2D6-expressing cells, the highest levels of MPDP (7.6 nmol/mg protein) and MPP^+ (1.3 nmol/mg protein) were found in −SRP CYP2D6-expressing cells (Table 1). These values were closer to the level of metabolites formed with rat brain mitochondria, which showed the highest levels (Table 1). The WT CYP2D6-expressing cells showed levels intermediary between −SRP and +SRP CYP2D6-expressing cells (Table 1).

As shown in Fig. 4*A*, the CYP contents of the mitochondrial and microsomal isolates measured by CO differential spectra varied markedly. The WT CYP2D6-expressing cells showed CYP contents of 0.6 nmol/mg for mitochondria and 0.8 nmol/mg protein for microsomes. For +SRP CYP2D6-expressing cells, the mitochondrial content was about 0.27 nmol/mg, whereas the microsomal content was 0.95 nmol/mg protein. In contrast, −SRP CYP2D6-expressing cells showed high mitochondrial CYP content (0.99 nmol/mg) and very low microsomal content, which was close to the mock-transfected cells. Because of the limited CYP contents of different subcellular fractions in some cells, a direct comparison of the microsomal and mitochondrial CYPs for the rates of metabolism of MPTP and bufuralol was not possible using these cell fractions. As shown in Fig. 4, *B* and *C*, the microsomal enzymes from the WT and +SRP CYP2D6-expressing cells exhibited nearly identical turnover number for bufuralol 1′-hydroxylation, and the mitochondrial enzymes from the WT and −SRP 2D6-expressing cells showed a comparable turnover number for MPP^+ formation (~1.2–1.3 nmol/min/nmol P450). It is therefore likely that

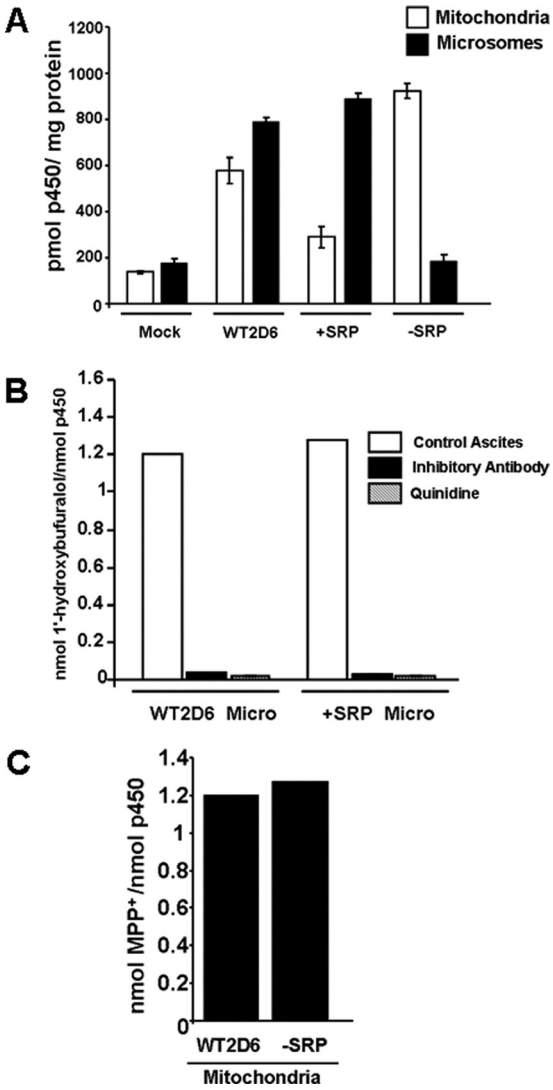

FIGURE 4. **Cytochrome P450 contents and metabolic activities of mitochondrial and microsomal fractions from stable Neuro-2A cells.** *A*, ferrous-CO *versus* ferrous difference spectra of mitochondria and microsomes of Neuro-2A cells. The P450 contents of mitochondrial and microsomal isolates were determined by using the dithionite-reduced and CO-bound difference spectra as described under "Materials and Methods." *B*, bufuralol 1′-hydroxylation activity of microsomal 2D6 from WT and +SRP 2D6-expressing cells. Enzyme reconstitution and reaction conditions to ensure first-order rate kinetics were as described by Hanna *et al.* (17). Microsomes (*Micro*) from −SRP 2D6-expressing cells could not be used because of low CYP content. The values represent the mean of two separate estimates. Inhibition studies were performed by preincubating enzymes for 20 min on ice with 10 μl of 2D6 inhibitory antibody (10 mg of protein/ml, BD Gentest, BD Biosciences) or 10 μM quinidine and 10 μM pargyline at 37 °C for 20 min. *C*, MPTP oxidation by mitochondria from WT and −SRP 2D6-expressing Neuro-2A cells. Enzyme reconstitution was carried out as described under "Materials and Methods" in the presence of added Adx +Adr. Mitochondria from +SRP-expressing cells were not used because of lower than desirable levels of CYP content. The values represent means of duplicate reactions.

the difference in the activities of the mitochondrial *versus* microsomal enzymes for MPTP metabolism is largely due to the difference in the electron transport proteins rather than the mutations targeted to the N-terminal signal domains.

Effects of MPTP on Complex I Activity and ROS Production in Neuro-2A Cells—All of the cell lines, including the mock-transfected cells, generated similar levels of ROS as measured by the Amplex Red method (Fig. 5*A*). The addition of MPTP induced

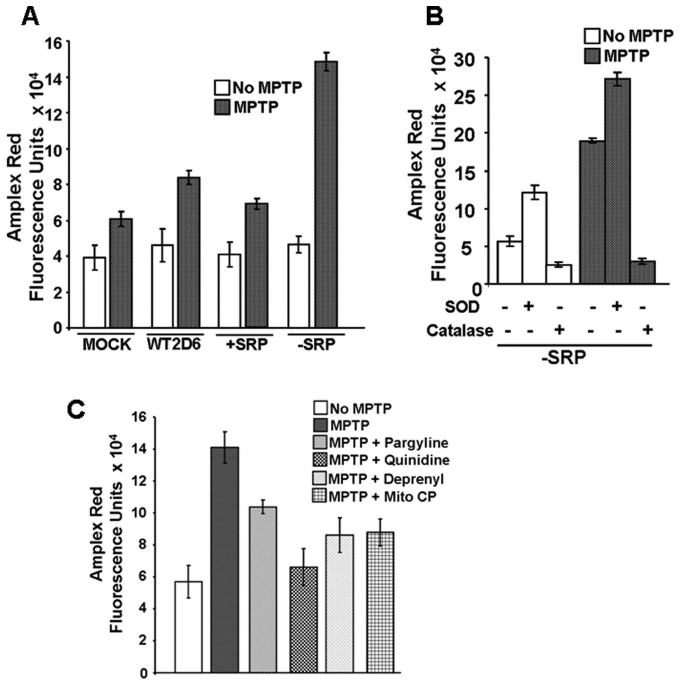

FIGURE 5. **MPTP-mediated ROS production in Neuro-2A cells stably expressing CYP2D6.** Stable Neuro-2A cells were grown with or without added MPTP (400 μM) and/or CYP2D6-specific inhibitor quinidine (10 μM) or a mitochondrion-specific antioxidant, mito-CP (0.5 μM). *A*, extracellular H_2O_2 levels were measured using the Amplex Red method as described under "Materials and Methods" in mock, WT2D6, +SRP, and −SRP cells. MPTP treatment (400 μM) was carried out for 48 h. *B*, effect of superoxide dismutase (*SOD*) and catalase on ROS in −SRP cells treated with or without MPTP *C*, effect of different inhibitors/antioxidant on ROS production in −SRP cells. 10 μM quinidine, deprenyl, and pargyline and 0.5 μM of mito-CP were used. MPTP treatment was as in *A*. Values represent the means ± S.E. of four separate assays.

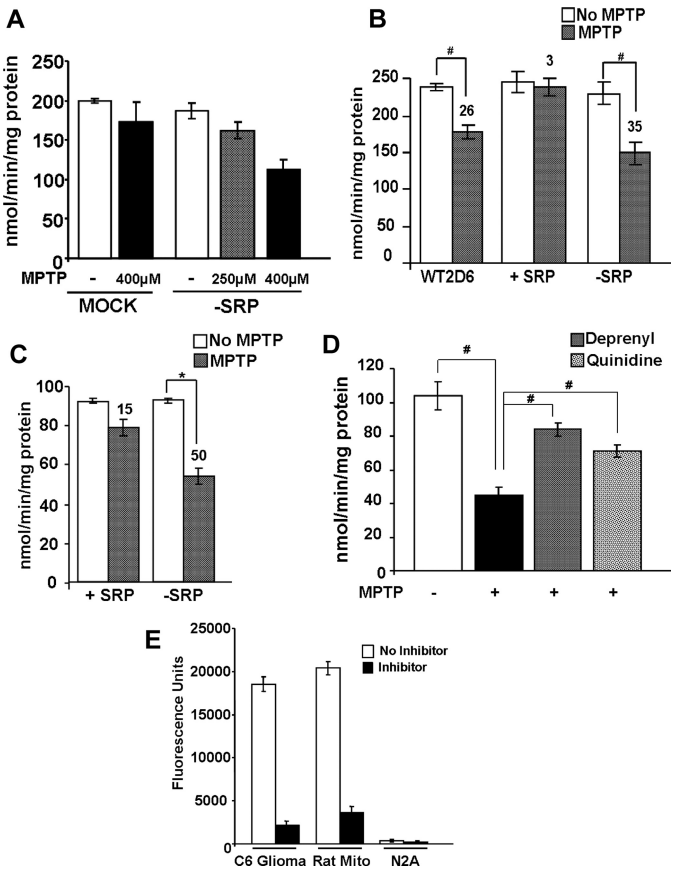

FIGURE 6. **Inhibition of mitochondrial complex I (NADH oxidoreductase) activity following exposure to MPTP.** *A* and *B*, complex I activity was measured in mitochondria isolated from undifferentiated Neuro-2A cells (50 μg of protein each) treated with or without MPTP. *Numbers* over the bar diagram in *B* show % inhibition by added MPTP compared with the nontreated control cells. *C*, complex I activity was measured in mitochondria from differentiated Neuro-2A cells expressing different *CYP2D6* cDNAs. Assays were run as in *A*. Effects of the CYP2D6-selective inhibitor quinidine (10 μM) and the MAO-B inhibitor deprenyl (10 μM) on complex I activity in mitochondria of −SRP cells were tested. *D*, inhibition of complex I in cells expressing −SRP 2D6. *E*, MAO activity was measured in mitochondria from rat liver, C6 glioma, and Neuro-2A cells using Amplex® Red monoamine oxidase assay kit, as per the manufacturer's protocol. Fluorometric assay of MAO-B was carried out using benzylamine as the substrate, based on the extent of inhibition by MAO-B inhibitor pargyline (10 μM). The activity was measured with 530 nm excitation and 590 nm emission. Results represent mean ± S.E. from three separate assays. * denotes $p < 0.05$ and # denotes $p < 0.001$.

ROS production in all cells. The increased ROS production (even in control cells) is consistent with previous reports suggesting inhibitory effects of MPTP on mitochondrial respiration (40). The rate of ROS production, however, was significantly higher in cells expressing −SRP CYP2D6, which is preferentially targeted to mitochondria. By contrast, ROS production in response to added MPTP was lowest in +SRP CYP2D6-expressing cells. In control experiments (Fig. 5*B*) treatment with the cell-permeable superoxide dismutase increased the Amplex Red signal, suggesting that these cells produce significant levels of $O_2^{\cdot-}$. The addition of cell-permeable superoxide dismutase markedly increased the MPTP-mediated increase in fluorescence signal, suggesting a high level of $O_2^{\cdot-}$ production in the treated cells (Fig. 5*B*). As expected, treatment with the cell-permeable catalase markedly reduced the signal, suggesting that the fluorescence signal is indeed due to H_2O_2 production. ROS production in −SRP 2D6-expressing cells was attenuated by the mitochondrion-targeted antioxidant mito-CP and also the CYP2D6 inhibitor quinidine (Fig. 5*C*), further confirming a role for mitochondrion-targeted CYP2D6 in MPTP-induced ROS production.

MPTP inhibited complex I activity in both undifferentiated and differentiated neurons (Fig. 6, *A* and *C*). MPTP inhibited complex I activity in mock-transfected cells only marginally, although the inhibition was quite notable (~45%) in −SRP 2D6-expressing cells (Fig. 6*A*). The inhibition was concentration-dependent, *i.e.* 250 μM MPTP was marginally effective in complex I inhibition. MPTP-mediated inhibition was highest in −SRP 2D6-expressing cells, moderately high in WT 2D6-expressing cells, and not visible in +SRP 2D6-expressing cells (Fig. 6*B*). The extent of MPTP-mediated complex I inhibition was highest (~50%) in differentiated Neuro-2A cells expressing −SRP 2D6 (Fig. 6*C*). Both quinidine and deprenyl restored the MPTP-mediated inhibition of complex I activity in −SRP 2D6-expressing cells (Fig. 6*D*). The MPTP-mediated inhibition was due to mitochondrial CYP2D6 because Neuro-2A cell mitochondria did not contain any measurable MAO activity. Thus, mitochondrion-targeted CYP2D6 potentiated MPTP metabolism and mitochondrial toxicity through the production of MPP^+. Complex IV and other electron transfer chain complexes were not affected significantly by these treatments (results not shown).

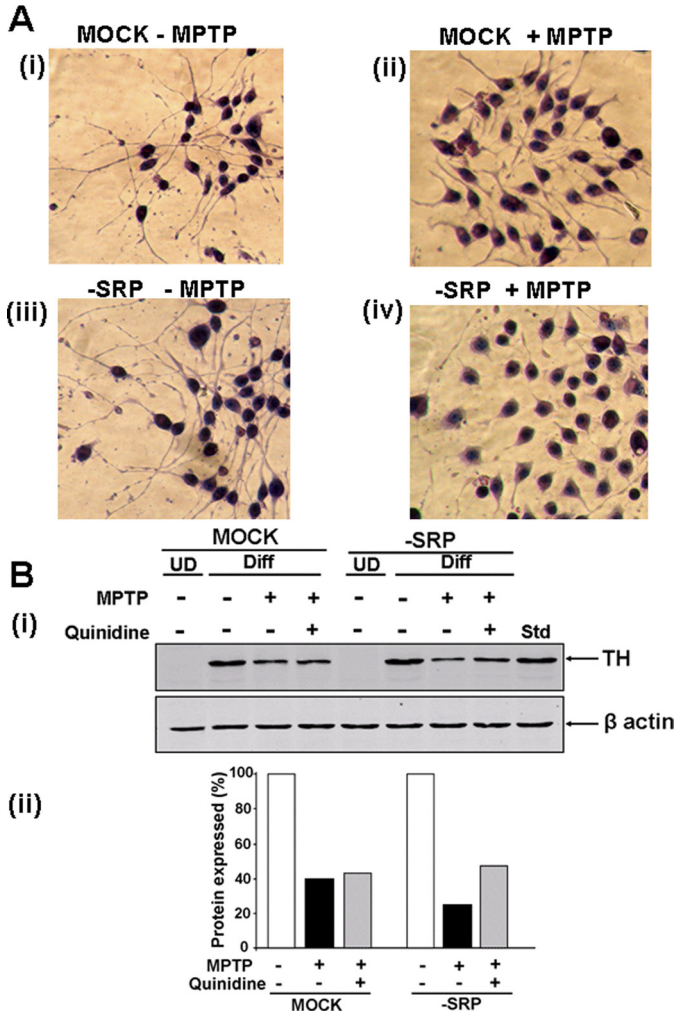

FIGURE 7. **Effects of MPTP on the differentiation of Neuro-2A cells expressing mitochondrion-targeted CYP2D6.** Neuro-2A cells were induced to differentiate for 72 h with 1 mM dibromo-cAMP. In some plates, MPTP (400 μM) was added after 24 h of differentiation. At the end of treatment, cells were fixed in ice-cold methanol, stained with hematoxylin and eosin, and viewed through an Olympus upright microscope. *A*, effects of MPTP on differentiated state of Neuro-2A cells. *Panels i* and *ii,* mock-transfected cells, without and with MPTP, respectively. *Panels iii* and *iv*, −SRP CYP2D6-expressing cells treated without and with MPTP, respectively. *B*, immunoblot of whole cell extracts (50 μg each) with antibody to TH (1:2000 dilution, v/v) (Immuno StAR, Hudson, WI). Blots for cell lysate were co-developed with antibody to actin (1:5000 dilution, v/v; Abcam, Cambridge, MA) as loading control. *Panel ii* shows quantitation of the immunoblot probed with TH antibody. *UD,* undifferentiated; *Diff,* differentiated.

MPTP-mediated Inhibition of Neuronal Differentiation and Induction of Autophagy Markers in −SRP 2D6-expressing Cells—The consequence of mitochondrial CYP2D6-induced MPTP metabolism on protein kinase A (PKA)-induced differentiation of Neuro-2A cells was studied by staining cells with hematoxylin and eosin. Both mock-transfected and −SRP 2D6-expressing cells underwent efficient differentiation in response to added cAMP and no MPTP, as seen by long and extensive axonal growth (Fig. 7*A*, *panel i,* and *panel iii*). The addition of MPTP marginally affected the differentiation of mock-transfected cells (Fig. 7*A*, *panel ii*). In contrast, cells stably expressing −SRP 2D6 showed blunted differentiation and axon growth in response to added MPTP (Fig. 7*A*, *panel iv*). These results suggest that metabolism of MPTP by mitochondrion-targeted CYP2D6 affects neuronal differentiation.

Consistent with the results in Fig. 7*A*, steady state levels of TH also varied in these cells. Immunoblots of total cell extracts (Fig. 7*B*) showed that TH, a well known marker for differentiation of dopaminergic neurons, is induced by serum deprivation or treatment with Bt_2cAMP for 3 days. MPTP treatment of mock-transfected cells resulted in marginal reduction in TH levels, which were not enhanced by treatment with quinidine. In contrast, MPTP treatment of primarily mitochondrion-targeted CYP2D6-expressing cells resulted in 70–80% inhibition, which was significantly reversed by treatment with quinidine. These results further confirm that MPTP oxidation by mitochondrion-targeted CYP2D6 contributes to mitochondrial toxicity and neuronal function.

We also investigated mitochondrial dynamics and autophagy in response to MPTP using immunohistochemical analysis of Neuro-2A cells. Parkin, which is recruited to mitochondria by the action of Pink-1, is an important marker for mitochondrial autophagy (41, 42). In this study, co-localization of Parkin with mitochondrial genome-coded cytochrome oxidase subunit 1 was used as a measure of mitochondrial localization. MPTP treatment of mock-transfected cells produced a marginal increase in mitochondrial localization of Parkin (Fig. 8*A*, *left panel*) which was not altered by treatment with the CYP2D6 inhibitor quinidine (Fig. 8*A*, *bottom panel*). In −SRP 2D6-expressing cells, however, MPTP treatment markedly increased mitochondrial localization of Parkin (Pearson coefficient 0.91; Fig. 8*B*), which was substantially reduced by treatment with quinidine (Fig. 8*B, bottom panel*). These results demonstrated that metabolic activity of mitochondrial CYP2D6 is critical for MPTP-induced recruitment of Parkin to the mitochondrial compartment.

Drp-1 is a protein involved in mitochondrial dynamics and induces mitochondrial fission as part of quality control during cell division, also during mitochondrial stress (43). The mitochondrial Drp-1 level in mock-transfected control cells was relatively low (Fig. 9*A*, *panel i*), which increases significantly by MPTP treatment (Fig. 9*A*, *panel ii*). Treatment with quinidine did not affect the MPTP-induced Drp-1 levels (Fig. 9*A*, *panel iii*). Cells expressing −SRP CYP2D6 also contained relatively low mitochondrial Drp-1 (Fig. 9*B*, *panel i*), which was increased by treatment with MPTP (Fig. 9*B*, *panel ii*, Pearson's coefficient 0.9). Treatment with quinidine, however, significantly reduced the MPTP-induced mitochondrial Drp-1 level (Fig. 9*B, panel iii*). These results show that MPTP induced mitochondrial localization of Drp-1 as part of mitochondrial stress, which was partly relieved by CYP2D6 inhibitor quinidine. These results together show that mitochondrial CYP2D6 plays a critical role in MPTP-induced mitochondrial dysfunction and autophagy.

Effects of MPTP on Primary Cortical Neurons—Because the mouse is an effective model for studying MPTP-induced Parkinson disease, we determined the effects of MPTP on the primary cortical neurons from mouse brain. These neurons are known to be a mixed population consisting of glutaminergic and GABAergic neurons (44). We evaluated cell death in control, MPTP-treated, and MPTP + quinidine-treated cells by trypan blue staining method. The trypan blue-positive cells

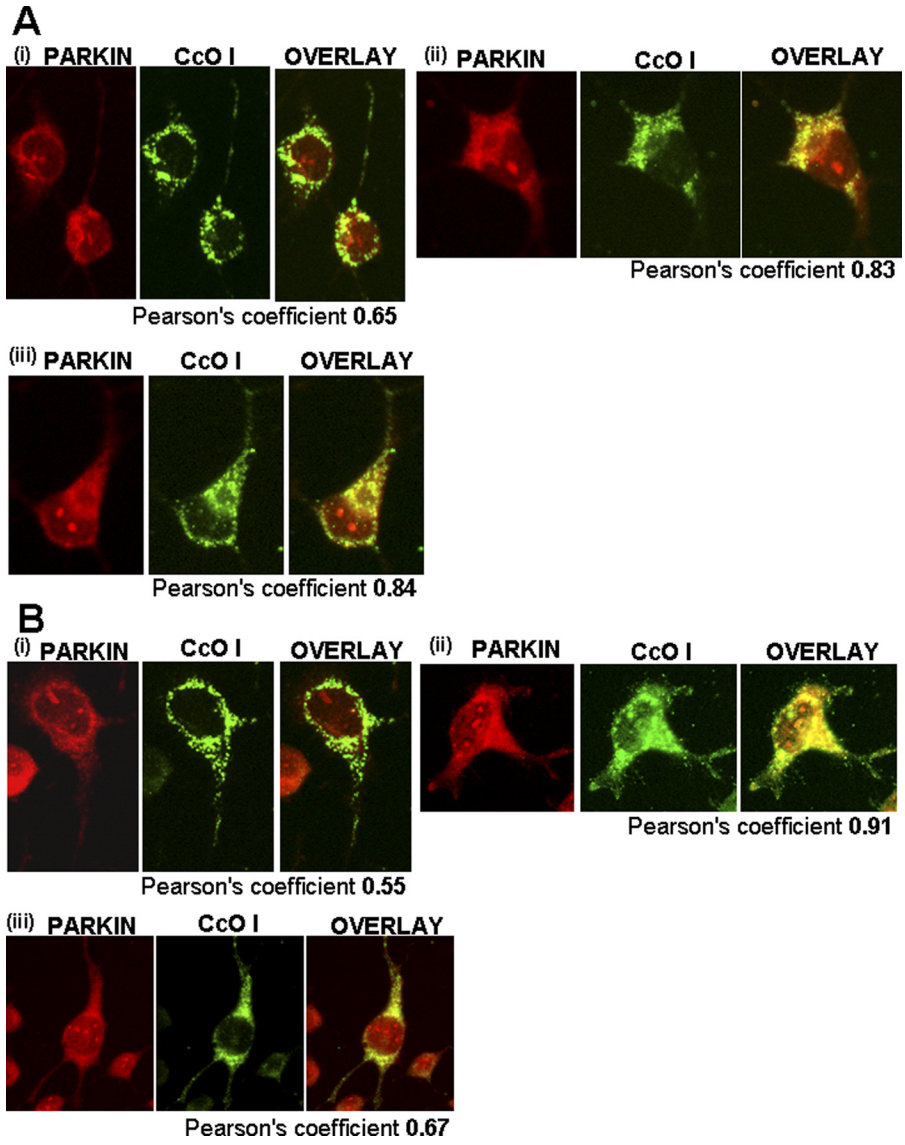

FIGURE 8. **Effects of MPTP on mitochondrial localization of autophagy marker, Parkin.** Immunofluorescence microscopy was carried out in differentiated Neuro-2A (Mock and −SRP cells) with and without added MPTP (400 μM) for 48 h and the CYP2D6-selective inhibitor quinidine (10 μM). Cells were incubated with a 1:1000 dilution (v/v) of primary anti-rabbit antibody to Parkin (Abcam, Cambridge, MA) and co-stained with a 1:500 dilution (v/v) of cytochrome oxidase I (anti-mouse) antibody as a mitochondrion-specific marker (Abcam, Cambridge, MA). The cells were subsequently incubated with Alexa 546-conjugated anti-rabbit and Alexa 488-conjugated anti-mouse IgG for colocalization of fluorescence signals. *A*, mock-transfected cells; *B*, −SRP 2D6-expressing cells. *Panel i*, cells with no MPTP treatment; *panel ii*, cells with added MPTP; *panel iii*, cells with added MPTP and quinidine. *Numbers* indicate Pearson coefficients calculated using Volocity 5.3 software.

were quantified by manual cell counting from six randomized fields/well. As shown in Fig. 10, *A* and *B*, there was an ~15% of cell death in control untreated cells, which was increased to 35% in MPTP-treated cells. Quinidine, a CYP2D6 inhibitor, reduced the cell death to ~25% suggesting that mitochondrial CYP2D6 plays a role in MPTP-induced cell death.

Effects of MPTP on Primary Dopaminergic Neurons—It is known that the isolation procedure used here yields a neuronal population that contains ~3–4% dopaminergic types. The dopaminergic neurons express their characteristic marker, TH. As shown in Fig. 11, *i* and *ii*, the TH-positive neurons express CYP2D6, a significant fraction of which (Pearson's coefficient 0.74) co-localized with mitochondrion-specific CcO IV antibody stain (Fig 11*i*). Fig. 11*iii* shows the triple staining of dopaminergic neurons with CYP2D6 antibody (*red*), TH antibody (*blue*), and Mitotracker Green FM (*green*). It is seen that TH neurons express CYP2D6, some of which co-localized with the mitochondrion-specific Mitotracker Green stain (Fig 11*iii, last panel*).

Fig. 12 shows the effects of MPTP on the TH-positive neurons and the effects of CYP inhibitor quinidine and known MAO-B inhibitors pargyline and deprenyl. As shown in Fig. 12*B*, the neuronal morphology is markedly altered with shorter axonal outgrowths. This loss is prevented to a significant extent by quinidine but to a lesser extent by the known MAO-B inhibitors shown to have different levels of inhibition on mitochondrial CYP2D6-dependent metabolism of MPTP to MPP$^+$. Quantitation of cell counts in Fig 12*F* shows that a high number of cell deaths (~40%) occurred in TH neurons treated with MPTP, which was partly reversed by pargyline and deprenyl,

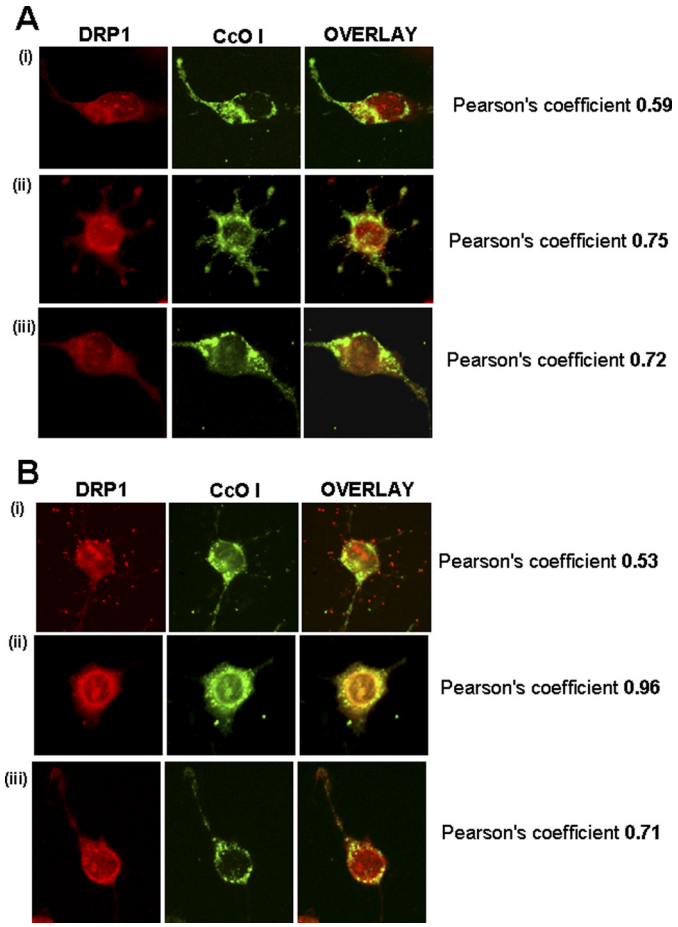

FIGURE 9. **Effects of MPTP on the induction of Drp-1, a marker for mitochondrial fission.** Immunofluorescence microscopy was carried out in differentiated Neuro-2A (mock and −SRP cells) with and without MPTP (400 μM) for 48 h as described in Fig. 7. Cells were incubated with a 1:250 dilution (v/v) of anti-rabbit DRP-1 antibody (Novus Biologicals, Littleton, CO) and co-stained with a 1:500 dilution (v/v) of cytochrome oxidase I (anti-mouse) antibody. The cells were subsequently incubated with Alexa 546-conjugated anti-rabbit and Alexa 488-conjugated anti-mouse IgG for co-localization of fluorescence signals. *A*, mock-transfected; *B*, −SRP CYP2D6-expressing cells. *Panel i*, cells with no MPTP treatment; *panel ii*, cells with MPTP treatment; *panel iii*, cells treated with MPTP and quinidine. *Numbers* indicate Pearson coefficients for co-localization, calculated using Volocity 5.3 software.

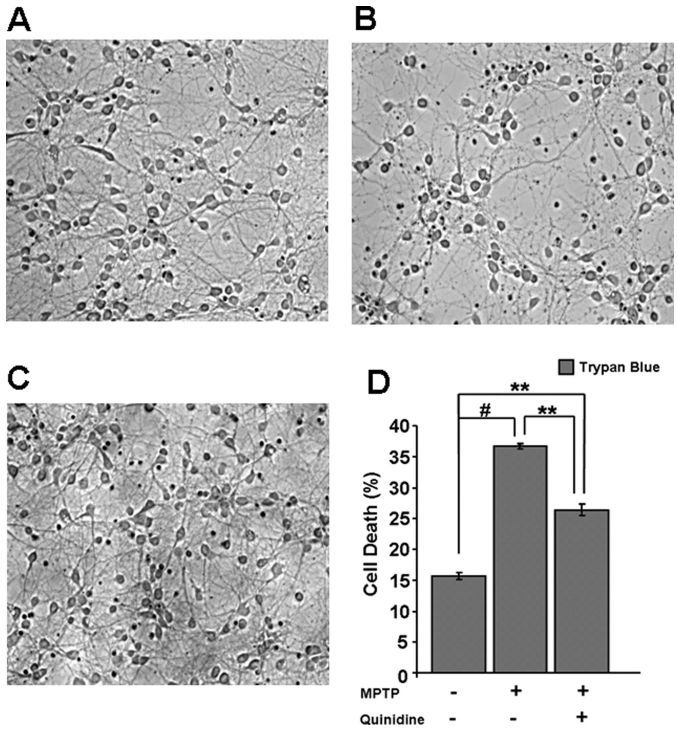

FIGURE 10. **Effect of MPTP treatment on primary mouse brain neurons.** Primary cortical neurons were seeded and grown for 8 days before treatment with MPTP and other agents for 48 h. Cell death was determined by trypan blue (0.4%) uptake by light microscopy (Nikon Eclipse TE 300) on ×20 magnification. *A*, trypan blue staining on neurons without any treatment; *B*, 50 μM MPTP treatment, and *C*, 50 μM MPTP plus 10 μM quinidine for 48 h. *D*, histogram representation of cell death (%) in control and treated groups. Isolation of primary neurons and counting methods were as described under "Materials and Methods." Mean values ± S.E. were calculated based on three separate measurement. ** denotes $p < 0.05$; # denotes $p < 0.001$.

but more effectively by quinidine. These results strongly suggest the *in vivo* relevance of our findings with cultured stably transduced Neuro-2A cells.

DISCUSSION

It is widely accepted that MAO-B (localized in the nondopaminergic neuronal cells and mostly of glial origin) is the major enzyme responsible for the toxic effects of neurotoxin, MPTP, through oxidative dehydrogenation to $MPDP^+$, which is subsequently oxidized to MPP^+. The current model for the MPTP-induced neuronal toxicity is presented in Fig. 13*A*. A convincing argument for this possibility was presented by experiments showing that MAO-B inhibitors (*e.g.* deprenyl and pargyline) rendered protection against MPTP and other neuroactive amines in rodents and primate models (1–3, 45, 46). In contrast to the current paradigm, our results show that mitochondrial CYP2D6 efficiently catalyzes the oxidation of MPTP to MPP^+ and that the catalytic activity of CYP2D6 is also inhibited by some of the well known inhibitors of MAO-B such as deprenyl and pargyline. These results therefore present a significant paradigm shift and suggest that mitochondrial CYP2D6 should be a focus of future drug design for treating or attenuating chemically induced Parkinson disease. An alternative model based on our present data is shown in Fig. 13*B*.

The inhibition of CYP2D6 activity by deprenyl and pargyline was an unexpected finding, given the widespread use of these drug as specific inhibitors of MAO-B in clinical settings. However, it has been reported that CYP2D6 is involved in the metabolism of deprenyl (36, 47–48), and deprenyl could therefore be acting as a competitive inhibitor of CYP2D6-mediated metabolism of MPTP. Deprenyl is also known to inhibit CYP2B1 and CYP1A1 (49, 50) and has been shown to inhibit aminopyrine *N*-demethylation activity in mouse brain slices (51). There are also several studies suggesting that deprenyl causes a decrease in total microsomal cytochrome P450 levels in liver and brain (50–52). The mechanism of inhibition by pargyline remains unclear and needs further investigation. Our results raise the question on the specificities of many of these inhibitors and suggest the need for a detailed evaluation of this problem.

In this study, we demonstrated that mitochondrial CYP2D6 can efficiently oxidize MPTP and that MPP^+ is the major product formed. Reconstitution of purified CYP2D6 enzyme with the mitochondrial electron transfer proteins Adx and Adr

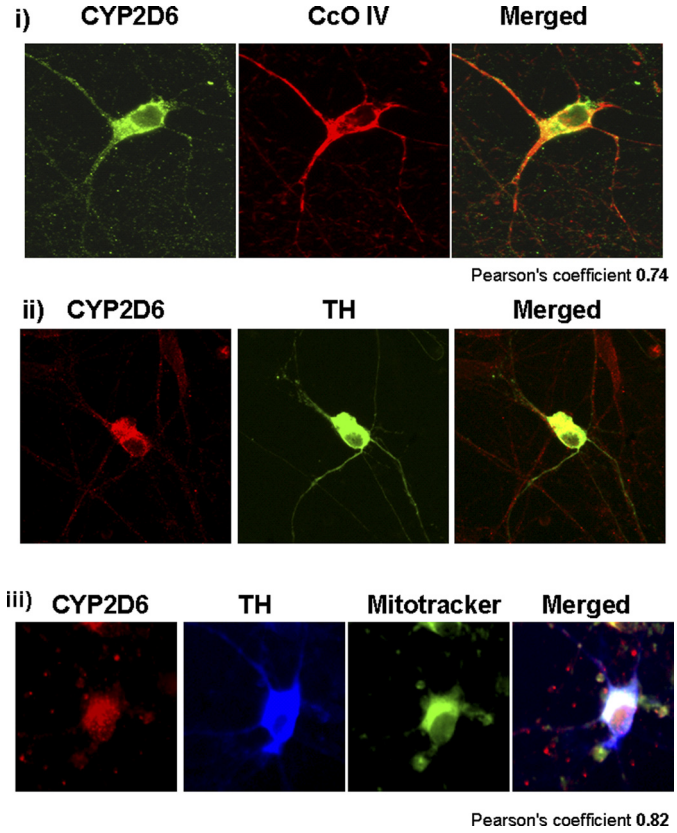

FIGURE 11. **Mitochondrial CYP2D6 localization in primary dopaminergic neurons.** Immunofluorescence microscopy was carried out as in Fig. 8 to identify localization of CYP2D6 in neuronal mitochondria. *i,* neurons were incubated with a 1:2000 dilution (v/v) of anti-mouse CYP2D6 antibody and co-stained with a 1:2000 dilution (v/v) of cytochrome oxidase subunit IVi1 (anti-rabbit) antibody. The cells were subsequently incubated with Alexa 488-conjugated anti-mouse and Alexa 546-conjugated anti-rabbit IgG for *green* and *red* fluorescence signals. *ii,* presence of CYP2D6 in dopaminergic neurons (TH) were detected by co-staining of anti-rabbit CYP2D6 (1:2000, Sigma) antibody (*red*) and anti-mouse tyrosine hydroxylase (1:1000) antibody (*green*). *iii,* triple staining was performed with anti-rabbit CYP2D6 antibody, Mitotracker Green (100 nM), and tyrosine hydroxylase antibody (*blue*) for verification of mitochondrial CYP2D6 localization. *Numbers* indicate Pearson coefficients for co-localization, calculated using Metamorph Advanced software.

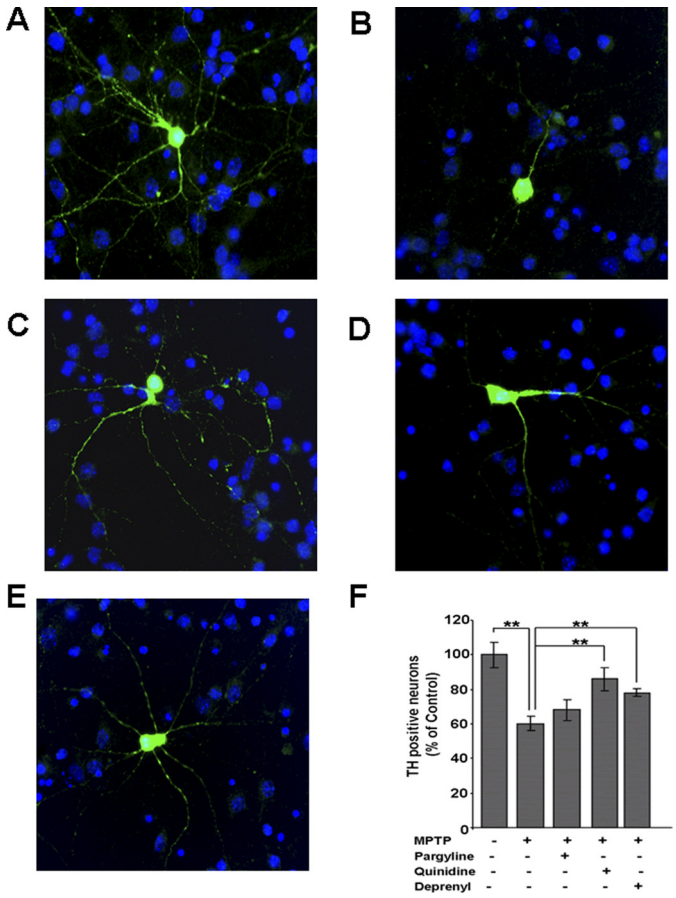

FIGURE 12. **Effects of MPTP on dopaminergic neurons.** Mesencephalic neurons cultured for 8 days were incubated with and without MPTP (50 μM) for 48 h. To assess the selective role of CYP2D6 in inducing MPTP-mediated toxicity, quinidine (10 μM), pargyline (5 μM), or deprenyl (10 μM) was added individually. Neurons were incubated with 1:1000 dilution of anti-mouse TH antibody, a marker for dopaminergic neurons and co-stained with DAPI (1 μg/ml). Emission from Alexa 488-conjugated anti-mouse IgG served as fluorescent signal. *A*, TH-stained dopaminergic neurons without treatment; *B*, neurons with MPTP treatment; *C*, neurons treated with MPTP and quinidine; *D*, neurons treated with MPTP and pargyline; *E*, neurons with MPTP and deprenyl (10 μM). *F*, presence of TH-positive neurons with treatments was determined as percentage of control (no treatment). Mean values ± S.E. was calculated based on three separate measurements. ** denotes $p < 0.05$.

resulted in the production of MPP^+ as the major metabolite. Likewise, production of MPP^+ by isolated mitochondria was significantly higher in cells expressing higher levels of mitochondrial CYP2D6 (Table 1). The formation of MPP^+ in CYP2D6-expressing mitochondria was inhibited by a CYP2D6 inhibitory antibody. In addition, MPTP-mediated inhibition of mitochondrial complex I activity required either expression of CYP2D6 in mitochondria or the addition of MAO-B to the reaction mixtures (data not shown). Together, these results suggest that mitochondrial CYP2D6 can contribute to MPTP-mediated mitochondrial toxicity.

Our results are of significance in view of previous data from our laboratory showing widely varying levels of mitochondrial CYP2D6 contents in human livers, ranging from relatively low to a major part of the hepatocellular pool (26, 37). Additionally, a study on the mitochondrial and microsomal distribution of CYP2D6 in different regions of human brain (28) showed that the substantia nigra, a region that is rich in dopaminergic neurons, contains the highest level of CYP2D6; also, the mitochondrial level of CYP2D6 in this brain region was nearly equal to or higher than in the microsomes (28). In support of our hypothesis, it was shown that CYP inhibitors such as piperonyl butoxide and SKF-525A significantly protected mouse brain slices from MPTP-mediated toxicity (51). In support of this, our results with primary cells not only show expression of CYP2D6 in dopaminergic neurons but also significant localization in the mitochondrial compartment (Fig. 12).

Several studies suggest that microsomal CYP2D6, supported by microsomal NPR, has a protective role through production of the inactive metabolites PTP and MPTP-OH, implying that higher microsomal CYP2D6 levels render a protective effect (53). In this regard, both WT and +SRP CYP2D6-expressing cells showed significantly less toxicity following MPTP treatment despite containing substantial albeit lower levels of mitochondrial CYP2D6 (Fig. 3*A*). Notably, these cell types also contain substantially higher levels of microsomal CYP2D6, which may be an important factor in their relative resistance to MPTP-induced toxicity (Figs. 3–5).

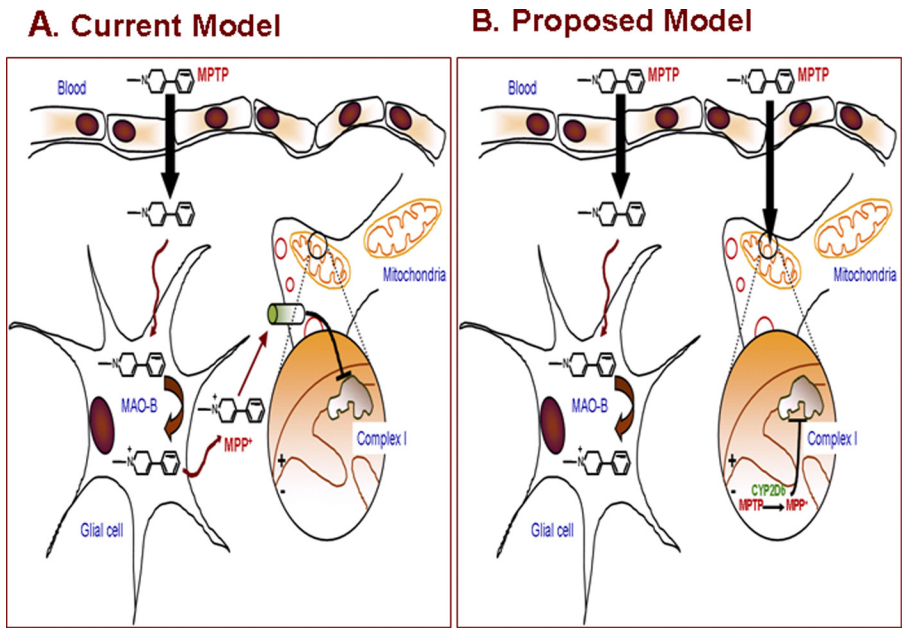

FIGURE 13. **Proposed new model for MPTP-mediated neurodegeneration.**

Although the molecular basis of altered MPTP metabolism by mitochondrial CYP2D6 in a Adx/Adr-supported system remains unclear, previous studies from our laboratory showed more open structures with lower α-helical contents for mitochondrion-targeted CYP1A1, -2E1, and -2B1 as judged by CD spectroscopy (54–57). Mitochondrial CYP1A1 exhibits high erythromycin *N*-demethylation activity and catalyzes the *N*-demethylation of at least five different neuroactive amine drugs that are not oxidized by the microsomal counterpart (56, 58–60). Also, mitochondrial CYP2E1 induced higher oxidative stress compared with microsomal CYP2E1 in response to alcohol treatment (61). At the same time, mitochondrial CYP1A1 exhibits markedly lower aryl hydrocarbon hydroxylase activity and elimination of hepatic benzo[*a*]pyrene as compared with microsomal CYP1A1 (62). It is also possible that the altered substrate specificity of microsomal cytochrome P450s bimodally targeted to mitochondria may be related to the different mechanism of electron transfer by the Adx/Adr system. The differences in the electron transfer systems between mitochondria and microsomes could cause different kinetics of electron transfer or different routes of electron flow, which may differentially modulate the catalytic activities of the cytochrome P450 enzymes.

Although there is no question that MAO-B localized on the outer membrane of nondopaminergic cells has high catalytic activity for MPTP metabolism, it is not clear how a highly toxic metabolite with a net positive charge could be transported out of cells instead of being transported into the mitochondrial matrix by virtue of its charge. Synthetic compounds of this type of charge property form steep gradients, with high level of accumulation in mitochondria (63) and progressively lower levels in the cytosol and extracellular compartments. Based on this, we propose an alternative model (Fig. 13) in which MPTP is transported into dopaminergic neurons, and once inside the cells, this highly lipophilic compound enters the mitochondrial compartment without the need for a transporter. MPP^+ formed inside the mitochondrial compartment is retained by mitochondria because of its positive charge, and the compound binds to and inhibits complex I activity.

In keeping with the results on significantly altered respiratory controls (Fig. 3), higher levels of ROS production (Fig. 5), and complex I inhibition (Fig. 6) in mitochondrial CYP2D6-expressing cells in response to added MPTP, these cells also show impaired neuronal differentiation and markers of altered mitochondrial dynamics and mitophagy (Figs. 7–9). The ubiquitin ligase Parkin is thought to be a marker for early onset of Parkinson disease (64, 65). Some models propose that Parkin is recruited by dysfunctional mitochondria (with disrupted $\Delta\psi_m$), where it induces the autophagic process (64). Consistent with this model, our results show that MPTP induces the localization of Parkin in Neuro-2A cell mitochondria. The localization is markedly increased in cells expressing mitochondrial CYP2D6 (Fig. 8). The dynamin-like GTPase Drp-1 is an important component of mitochondrial fission machinery (66). It has been proposed that extensive mitochondrial fission is a marker for mitochondrial stress and even apoptosis (67). Increased mitochondrial localization of Drp-1 in mitochondrial CYP2D6-expressing cells in response to MPTP treatment (Fig. 9) provides additional evidence for increased mitochondrial stress in these cells. A key point of this study is the reversal of MPTP-mediated mitochondrial dysfunction, ROS production, and appearance of autophagy markers in predominantly mitochondrial CYP2D6-expressing cells by added quinidine, which implicates a direct role for mitochondrial CYP2D6 in potentiating the toxic effects of the pro-neurotoxin. Our results also show that primary dopaminergic neurons expressing mitochondrial CYP2D6 show blunted axon extensions and cell death when exposed to MPTP, which is attenuated by the CYP2D6-specific inhibitor quinidine. These results suggest that our observations on the role of mitochondrial CYP2D6 are physiologically significant.

For the first time, we provide evidence that the activation of MPTP and other biogenic amines occurs within the mitochondrial compartment of dopaminergic neurons. The CYP2D6 inhibitor quinidine not only inhibited MPTP metabolism but also attenuated MPTP-mediated complex I inhibition, ROS production, and progression of mitochondrial autophagy. We propose that human mitochondrial CYP2D6 potentiates MPTP-mediated mitochondrial dysfunction in dopaminergic neurons, the cause of neuronal degeneration in this model of Parkinson disease (68).

Acknowledgments—We thank Dr. B. Kalyanaraman (University of Wisconsin, Milwaukee) for providing the MitoQ and Mito-CP used in this study. We also thank members of the Avadhani laboratory for many constructive suggestions.

REFERENCES

1. Kopin, I. J., and Markey, S. P. (1988) MPTP toxicity. Implications for research in Parkinson disease. *Annu. Rev. Neurosci.* **11,** 81–96
2. Meredith, G. E., Sonsalla, P. K., and Chesselet, M. F. (2008) Animal models of Parkinson disease progression. *Acta Neuropathol.* **115,** 385–398
3. Sonsalla, P. K., and Heikkila, R. E. (1986) The influence of dose and dosing interval on MPTP-induced dopaminergic neurotoxicity in mice. *Eur. J. Pharmacol.* **129,** 339–345
4. Chiba, K., Trevor, A., and Castagnoli, N., Jr. (1984) Metabolism of the neurotoxic tertiary amine, MPTP, by brain monoamine oxidase. *Biochem. Biophys. Res. Commun.* **120,** 574–578
5. Chiba, K., Peterson, L. A., Castagnoli, K. P., Trevor, A. J., and Castagnoli, N., Jr. (1985) Studies on the molecular mechanism of bioactivation of the selective nigrostriatal toxin 1-methyl-4-phenyl-1,2,3,6-tetrahydropyridine. *Drug Metab. Dispos.* **13,** 342–347
6. Przedborski, S., Tieu, K., Perier, C., and Vila, M. (2004) MPTP as a mitochondrial neurotoxic model of Parkinson disease. *J. Bioenerg. Biomembr.* **36,** 375–379
7. Bezard, E., Gross, C. E., Fournier, M. C., Dovero, S., Bloch, B., and Jaber, M. (1999) Absence of MPTP-induced neuronal death in mice lacking the dopamine transporter. *Exp. Neurol.* **155,** 268–273
8. Ramsay, R. R., Dadgar, J., Trevor, A., and Singer, T. P. (1986) Energy-driven uptake of *N*-methyl-4-phenylpyridine by brain mitochondria mediates the neurotoxicity of MPTP. *Life Sci.* **39,** 581–588
9. Ramsay, R. R., Kowal, A. T., Johnson, M. K., Salach, J. I., and Singer, T. P. (1987) The inhibition site of MPP$^+$, the neurotoxic bioactivation product of 1-methyl-4-phenyl-1,2,3,6-tetrahydropyridine is near the Q-binding site of NADH dehydrogenase. *Arch. Biochem. Biophys.* **259,** 645–649
10. Di Monte, D., Jewell, S. A., Ekström, G., Sandy, M. S., and Smith, M. T. (1986) Methyl-4-phenyl-1,2,3,6-tetrahydropyridine (MPTP) and 1-methyl-4-phenylpyridine (MPP$^+$) cause rapid ATP depletion in isolated hepatocytes. *Biochem. Biophys. Res. Commun.* **137,** 310–315
11. Hasegawa, E., Takeshige, K., Oishi, T., Murai, Y., and Minakami, S. (1990) Methyl-4-phenylpyridinium (MPP$^+$) induces NADH-dependent superoxide formation and enhances NADH-dependent lipid peroxidation in bovine heart submitochondrial particles. *Biochem. Biophys. Res. Commun.* **170,** 1049–1055
12. Rossetti, Z. L., Sotgiu, A., Sharp, D. E., Hadjiconstantinou, M., and Neff, N. H. (1988) 1-Methyl-4-phenyl-1,2,3,6-tetrahydropyridine (MPTP) and free radicals *in vitro*. *Biochem. Pharmacol.* **37,** 4573–4574
13. Bloem, B. R., Irwin, I., Buruma, O. J., Haan, J., Roos, R. A., Tetrud, J. W., and Langston, J. W. (1990) The MPTP model. Versatile contributions to the treatment of idiopathic Parkinson disease. *J. Neurol. Sci.* **97,** 273–293
14. Siegle, I., Fritz, P., Eckhardt, K., Zanger, U. M., and Eichelbaum, M. (2001) Cellular localization and regional distribution of CYP2D6 mRNA and protein expression in human brain. *Pharmacogenetics* **11,** 237–245
15. Coleman, T., Ellis, S. W., Martin, I. J., Lennard, M. S., and Tucker, G. T. (1996) 1-Methyl-4-phenyl-1,2,3,6-tetrahydropyridine (MPTP) is *N*-demethylated by cytochromes P450 2D6, 1A2, and 3A4—implications for susceptibility to Parkinson disease. *J. Pharmacol. Exp. Ther.* **277,** 685–690
16. Gilham, D. E., Cairns, W., Paine, M. J., Modi, S., Poulsom, R., Roberts, G. C., and Wolf, C. R. (1997) Metabolism of MPTP by cytochrome P4502D6 and the demonstration of 2D6 mRNA in human fetal and adult brain by *in situ* hybridization. *Xenobiotica* **27,** 111–125
17. Hanna, I. H., Kim, M. S., and Guengerich, F. P. (2001) Heterologous expression of cytochrome P450 2D6 mutants, electron transfer, and catalysis of bufuralol hydroxylation: the role of aspartate 301 in structural integrity. *Arch. Biochem. Biophys.* **393,** 255–261
18. Herraiz, T., Guillén, H., Arán, V. J., Idle, J. R., and Gonzalez, F. J. (2006) Comparative aromatic hydroxylation and *N*-demethylation of MPTP neurotoxin and its analogs, *N*-methylated β-carboline and isoquinoline alkaloids, by human cytochrome P450 2D6. *Toxicol. Appl. Pharmacol.* **216,** 387–398
19. Modi, S., Gilham, D. E., Sutcliffe, M. J., Lian, L. Y., Primrose, W. U., Wolf, C. R., and Roberts, G. C. (1997) *N*-Methyl-4-phenyl-1,2,3,6-tetrahydropyridine as a substrate of cytochrome P450 2D6. Allosteric effects of NADPH-cytochrome P450 reductase. *Biochemistry* **36,** 4461–4470
20. Narimatsu, S., Tachibana, M., Masubuchi, Y., and Suzuki, T. (1996) Mutant debrisoquine hydroxylation genes in Parkinson disease. *Chem. Res. Toxicol.* **9,** 93–98
21. Gołab-Janowska, M., Honczarenko, K., Gawrońska-Szklarz, B., and Potemkowski, A. (2007) A *CYP2D6* gene polymorphism as a probable risk factor for Alzheimer's disease and Parkinson's disease with dementia. *Neurol. Neurochir. Pol.* **41,** 113–121
22. Smith, C. A., Gough, A. C., Leigh, P. N., Summers, B. A., Harding, A. E., Maraganore, D. M., Sturman, S. G., Schapira, A. H., Williams, A. C., and Maranganore, D. M. (1992) Debrisoquine hydroxylase gene polymorphism and susceptibility to Parkinson disease. *Lancet* **339,** 1375–1377
23. Halling, J., Petersen, M. S., Grandjean, P., Weihe, P., and Brosen, K. (2008) Genetic predisposition to Parkinson disease. *CYP2D6* and HFE in the Faroe Islands. *Pharmacogenet. Genomics* **18,** 209–212
24. Kallio, J., Marttila, R. J., Rinne, U. K., Sonninen, V., and Syvälahti, E. (1991) Debrisoquine oxidation in Parkinson disease. *Acta Neurol. Scand.* **83,** 194–197
25. Persad, A. S., Stedeford, T., Tanaka, S., Chen, L., and Banasik, M. (2003) Parkinson disease and *CYP2D6* polymorphism in Asian populations. A meta-analysis. *Neuroepidemiology* **22,** 357–361
26. Sangar, M. C., Anandatheerthavarada, H. K., Tang, W., Prabu, S. K., Martin, M. V., Dostalek, M., Guengerich, F. P., and Avadhani, N. G. (2009) Human liver mitochondrial cytochrome P450 2D6—individual variations and implications in drug metabolism. *FEBS J.* **276,** 3440–3453
27. Sangar, M. C., Bansal, S., and Avadhani, N. G. (2010) Bimodal targeting of microsomal cytochrome P450s to mitochondria: implications in drug metabolism and toxicity. *Expert Opin. Drug Metab. Toxicol.* **6,** 1231–1251
28. Dutheil, F., Dauchy, S., Diry, M., Sazdovitch, V., Cloarec, O., Mellottée, L., Bièche, I., Ingelman-Sundberg, M., Flinois, J. P., de Waziers, I., Beaune, P., Declèves, X., Duyckaerts, C., and Loriot, M. A. (2009) Xenobiotic metabolizing enzymes and transporters in the normal human brain. Regional and cellular mapping as a basis for putative roles in cerebral function. *Drug Metab. Dispos.* **37,** 1528–1538
29. Morgenstern, J. P., and Land, H. (1991) Choice and manipulation of retroviral vectors. *Methods Mol. Biol.* **7,** 181–206
30. Krajl, M. (1965) A rapid microfluorimetric determination of monoamine oxidase. *Biochem. Pharmacol.* **14,** 1684–1686
31. Lowry, O. H., Rosebrough, N. J., Farr, A. L., and Randall, R. J. (1951) Protein measurement with the Folin phenol reagent. *J. Biol. Chem.* **193,** 265–275
32. Wu, M., Neilson, A., Swift, A. L., Moran, R., Tamagnine, J., Parslow, D., Armistead, S., Lemire, K., Orrell, J., Teich, J., Chomicz, S., and Ferrick, D. A. (2007) Multiparameter metabolic analysis reveals a close link between attenuated mitochondrial bioenergetic function and enhanced glycolysis dependency in human tumor cells. *Am. J. Physiol. Cell Physiol.* **292,** C125–C136
33. Birch-Machin, M. A., and Turnbull, D. M. (2001) Assaying mitochondrial respiratory complex activity in mitochondria isolated from human cells and tissues. *Methods Cell Biol.* **65,** 97–117

34. Yamazaki, H., Nakamura, M., Komatsu, T., Ohyama, K., Hatanaka, N., Asahi, S., Shimada, N., Guengerich, F. P., Shimada, T., Nakajima, M., and Yokoi, T. (2002) Roles of NADPH-P450 reductase and apo- and holocytochrome b_5 on xenobiotic oxidations catalyzed by 12 recombinant human cytochrome P450s expressed in membranes of *Escherichia coli*. *Protein Expr. Purif.* **24,** 329–337
35. Omura, T., and Sato, R. (1964) The carbon monoxide-binding pigment of liver microsomes I. Evidence for its hemoprotein nature. *J. Biol. Chem.* **239,** 2370–2378
36. Guengerich, F. P. (1982) in *Principles and Methods of Toxicology* (Hayes, A. W., ed) pp. 609–634, Raven Press, Ltd., New York
37. Sangar, M. C., Anandatheerthavarada, H. K., Martin, M. V., Guengerich, F. P., and Avadhani, N. G. (2010) Identification of genetic variants of human cytochrome P450 2D6 with impaired mitochondrial targeting. *Mol. Genet. Metab.* **99,** 90–97
38. Grace, J. M., Kinter, M. T., and Macdonald, T. L. (1994) Atypical metabolism of deprenyl and its enantiomer, (*S*)-(+)-*N*,α-dimethyl-*N*-propynylphenethylamine, by cytochrome P450 2D6. *Chem. Res. Toxicol.* **7,** 286–290
39. Mizuno, Y., Suzuki, K., Sone, N., and Saitoh, T. (1988) Inhibition of mitochondrial respiration by 1-methyl-4-phenyl-1,2,3,6-tetrahydropyridine (MPTP) in mouse brain *in vivo*. *Neurosci. Lett.* **91,** 349–353
40. Clark, I. E., Dodson, M. W., Jiang, C., Cao, J. H., Huh, J. R., Seol, J. H., Yoo, S. J., Hay, B. A., and Guo, M. (2006) *Drosophila* pink1 is required for mitochondrial function and interacts genetically with parkin. *Nature* **441,** 1162–1166
41. Murphy, A. N. (2009) In a flurry of PINK, mitochondrial bioenergetics takes a leading role in Parkinson disease. *EMBO Mol. Med.* **1,** 81–84
42. Arnoult, D. (2007) Mitochondrial fragmentation in apoptosis. *Trends Cell Biol.* **17,** 6–12
43. Kohutnicka, M., Lewandowska, E., Kurkowska-Jastrzebska, I., Członkowski, A., and Członkowska, A. (1998) Microglial and astrocytic involvement in a murine model of Parkinson disease induced by 1-methyl-4-phenyl-1,2,3,6-tetrahydropyridine (MPTP). *Immunopharmacology* **39,** 167–180
44. Molyneaux, B. J., Arlotta, P., Menezes, J. R., and Macklis, J. D. (2007) Neuronal subtype specification in the cerebral cortex. *Nat. Rev. Neurosci.* **8,** 427–437
45. Robertson, D. C., Schmidt, O., Ninkina, N., Jones, P. A., Sharkey, J., and Buchman, V. L. (2004). Developmental loss and resistance to MPTP toxicity of dopaminergic neurones in substantia nigra pars compacta of γ-synuclein, α-synuclein, and double α/γ-synuclein null mutant mice. *J. Neurochem.* **89,** 1126–1136
46. Bach, M. V., Coutts, R. T., and Baker, G. B. (2000) Metabolism of *N*,*N*-dialkylated amphetamines, including deprenyl, by CYP2D6 expressed in a human cell line. *Xenobiotica* **30,** 297–306
47. Dragoni, S., Bellik, L., Frosini, M., Sgaragli, G., Marini, S., Gervasi, P. G., and Valoti, M. (2003) L-Deprenyl metabolism by the cytochrome P450 system in monkey (*Cercopithecus aethiops*) liver microsomes. *Xenobiotica* **33,** 181–195
48. Rittenbach, K. A., and Baker, G. B. (2007) Involvement of cytochromes P450 2D6, 2B6, and 2C19 in the metabolism of (−)-deprenyl and *N*-methyl,*N*-propargylphenylethylamine. *Drug Metab. Lett.* **1,** 97–100
49. Dyck, L. E., and Davis, B. A. (2001) Inhibition of rat liver microsomal CYP1A2 and CYP2B1 activity by *N*-(2-heptyl)-*N*-methyl-propargylamine and by *N*-(2-heptyl)-propargylamine. *Drug Metab. Dispos.* **29,** 1156–1161
50. Sharma, U., Roberts, E. S., and Hollenberg, P. F. (1996) Inactivation of cytochrome P4502B1 by the monoamine oxidase inhibitors *R*-(−)-deprenyl and clorgyline. *Drug Metab. Dispos.* **24,** 669–675
51. Pai, K. S., and Ravindranath, V. (1991) Protection and potentiation of MPTP-induced toxicity by cytochrome P-450 inhibitors and inducer. *In vitro* studies with brain slices. *Brain Res.* **555,** 239–244
52. Valoti, M., Fusi, F., Frosini, M., Pessina, F., Tipton, K. F., and Sgaragli, G. P. (2000) Cytochrome P450-dependent *N*-dealkylation of L-deprenyl in C57BL mouse liver microsomes. Effects of *in vivo* pretreatment with ethanol, phenobarbital, β-naphthoflavone, and L-deprenyl. *Eur. J. Pharmacol.* **391,** 199–206
53. Mann, A., Miksys, S. L., Gaedigk, A., Kish, S. J., Mash, D. C., and Tyndale, R. F. (2012) The neuroprotective enzyme CYP2D6 increases in the brain with age and is lower in Parkinson disease patients. *Neurobiol. Aging* **33,** 2160–2171
54. Anandatheerthavarada, H. K., Addya, S., Dwivedi, R. S., Biswas, G., Mullick, J., and Avadhani, N. G. (1997) Bimodal targeting of cytochrome P450s to endoplasmic reticulum and mitochondria. The concept of chimeric signals. *Arch. Biochem. Biophys.* **339,** 136–150
55. Anandatheerthavarada, H. K., Addya, S., Mullick, J., and Avadhani, N. G. (1998) Localization of multiple forms of inducible cytochromes P450 in rat liver mitochondria. Immunological characteristics and patterns of xenobiotic substrate metabolism. *Biochemistry* **37,** 1150–1160
56. Avadhani, N. G., Sangar, M. C., Bansal, S., and Bajpai, P. (2011) Interaction of adrenodoxin with P4501A1 and its truncated form P450MT2 through different domains. Differential modulation of enzyme activities. *FEBS J.* **278,** 4218–4229
57. Robin, M. A., Anandatheerthavarada, H. K., Fang, J. K., Cudic, M., Otvos, L., and Avadhani, N. G. (2001) Mitochondrial targeted cytochrome P450 2E1 (P450 MT5) contains an intact N terminus and requires mitochondrial specific electron transfer proteins for activity. *J. Biol. Chem.* **276,** 24680–24689
58. Anandatheerthavarada, H. K., Vijayasarathy, C., Bhagwat, S. V., Biswas, G., Mullick, J., and Avadhani, N. G. (1999) Physiological role of the N-terminal processed P4501A1 targeted to mitochondria in erythromycin metabolism and reversal of erythromycin-mediated inhibition of mitochondrial protein synthesis. *J. Biol. Chem.* **274,** 6617–6625
59. Anandatheerthavarada, H. K., Amuthan, G., Biswas, G., Robin, M. A., Murali, R., Waterman, M. R., and Avadhani, N. G. (2001) Evolutionarily divergent electron donor proteins interact with P450MT2 through the same helical domain but different contact points. *EMBO J.* **20,** 2394–2403
60. Boopathi, E., Anandatheerthavarada, H. K., Bhagwat, S. V., Biswas, G., Fang, J. K., and Avadhani, N. G. (2000) Accumulation of mitochondrial P450MT2, NH_2-terminal truncated cytochrome P4501A1 in rat brain during chronic treatment with β-naphthoflavone. A role in the metabolism of neuroactive drugs. *J. Biol. Chem.* **275,** 34415–34423
61. Bansal, S., Liu, C. P., Sepuri, N. B., Anandatheerthavarada, H. K., Selvaraj, V., Hoek, J., Milne, G. L., Guengerich, F. P., and Avadhani, N. G. (2010) Mitochondria-targeted cytochrome P450 2E1 induces oxidative damage and augments alcohol-mediated oxidative stress. *J. Biol. Chem.* **285,** 24609–24619
62. Dong, H., Dalton, T. P., Miller, M. L., Chen, Y., Uno, S., Shi, Z., Shertzer, H. G., Bansal, S., Avadhani, N. G., and Nebert, D. W. (2009). Knock-in mouse lines expressing either mitochondrial or microsomal CYP1A1. Differing responses to dietary benzo[*a*]pyrene as proof of principle. *Mol. Pharmacol.* **75,** 555–567
63. Smith, R. A., Hartley, R. C., and Murphy, M. P. (2011) Mitochondria-targeted small molecule therapeutics and probes. *Antioxid. Redox Signal.* **15,** 3021–3038
64. Tanaka, A., Cleland, M. M., Xu, S., Narendra, D. P., Suen, D. F., Karbowski, M., and Youle, R. J. (2010) PINK1-dependent recruitment of Parkin to mitochondria in mitophagy. *J. Cell Biol.* **191,** 1367–1380
65. Vives-Bauza, C., Zhou, C., Huang, Y., Cui, M., de Vries, R. L., Kim, J., May, J., Tocilescu, M. A., Liu, W., Ko, H. S., Magrané, J., Moore, D. J., Dawson, V. L., Grailhe, R., Dawson, T. M., Li, C., Tieu, K., and Przedborski, S. (2010) Proteasome and p97 mediate mitophagy and degradation of mitofusins induced by Parkin. *Proc. Natl. Acad. Sci. U.S.A.* **107,** 378–383
66. Frank, S., Gaume, B., Bergmann-Leitner, E. S., Leitner, W. W., Robert, E. G., Catez, F., Smith, C. L., and Youle, R. J. (2001) The role of dynamin-related protein 1, a mediator of mitochondrial fission, in apoptosis. *Dev. Cell* **1,** 515–525
67. Arnoult, D., Rismanchi, N., Grodet, A., Roberts, R. G., Seeburg, D. P., Estaquier, J., Sheng, M., and Blackstone, C. (2005) Bax/Bak-dependent release of DDP/TIMM8a promotes Drp1-mediated mitochondrial fission and mitoptosis during programmed cell death. *Curr. Biol.* **15,** 2112–2118
68. Vila, M., and Przedborski, S. (2003) Targeting programmed cell death in neurodegenerative diseases. *Nat. Rev. Neurosci.* **4,** 365–375